

1 Historical (1960–2014) lightning and LNO_x trends and their 2 controlling factors in a chemistry–climate model

3 Yanfeng He¹, Kengo Sudo^{1,2}

4 ¹ Graduate School of Environment Studies, Nagoya University, Nagoya, 464-8601, Japan

5 ² Japan Agency for Marine–Earth Science and Technology (JAMSTEC), Yokohama, 237-0061, Japan

6 Correspondence to: Yanfeng He (hyf412694462@gmail.com)

7 **Abstract.** Lightning can cause natural ~~disasters~~hazards that ~~engender~~result in human and animal injuries or fatalities,
8 infrastructure destruction, and wildfire ignition. Lightning-produced NO_x (LNO_x), a major NO_x (NO_x=NO+NO₂) source, plays
9 a vital role in atmospheric chemistry and global climate. The Earth has experienced marked global warming and changes in
10 aerosol and aerosol precursor emissions (AeroPEs) since the 1960s. Investigating long-term historical (1960–2014) lightning
11 and LNO_x trends can provide important indicators for all lightning-related phenomena and for LNO_x effects on atmospheric
12 chemistry and global climate. Understanding how global warming and changes in AeroPEs influence historical lightning–
13 LNO_x trends ~~is also can be~~ helpful ~~because it can provide~~in providing a scientific basis for assessing future lightning–LNO_x
14 trends. Moreover, global lightning activities' responses to large volcanic eruptions (~~such as the 1991 Pinatubo eruption~~) are
15 not well elucidated, and are worth exploring. This study ~~used~~employed the widely used cloud top height lightning scheme
16 (CTH scheme) and the newly developed ice-based ECMWF-McCAUL lightning scheme to investigate historical (1960–2014)
17 lightning–LNO_x trends and variations and their ~~controlling~~influencing factors (global warming, increases in AeroPEs, and
18 Pinatubo eruption) in the framework of the CHASER (MIROC) chemistry–climate model. Results of ~~sensitive~~sensitivity
19 experiments indicate that both lightning schemes simulated almost flat global mean lightning flash rate trends during 1960–
20 2014 in CHASER. Moreover, both lightning schemes suggest that past global warming enhances historical trends of global
21 mean lightning density and global LNO_x emissions in a positive direction (around 0.03% yr⁻¹ or 3% K⁻¹). However, past
22 increases in AeroPEs exert an opposite effect to the lightning–LNO_x trends (-0.07% yr⁻¹ – -0.04% yr⁻¹ for lightning and -0.08%
23 yr⁻¹ – -0.03% yr⁻¹ for LNO_x) ~~when one considers only the aerosol radiative effects in the cumulus convection scheme.~~
24 Additionally, effects of past global warming and increases in AeroPEs on lightning trends were found to be heterogeneous
25 across different regions when analyzing lightning trends on the global map. Lastly, this ~~study report~~ is the first ~~to suggest of~~
26 ~~study results suggesting~~ that global lightning activities were suppressed markedly during the first year after the Pinatubo
27 eruption shown in both lightning schemes (global lightning activities decreased by as much as ~~17.02~~18.10% simulated by the
28 ECMWF-McCAUL scheme). Based on ~~the~~-simulated suppressed lightning activities after the Pinatubo eruption, ~~our~~
29 ~~study findings~~ also ~~indicates~~indicate that global LNO_x emissions decreased after the ~~2–3-year~~ Pinatubo eruption (~~2.41~~1.99%–
30 ~~8.72~~4.7% for the annual percentage reduction), ~~which lasted 2–3 years.~~ Model intercomparisons of lightning flash rate trends
31 and variations between our study (CHASER) and other Coupled Model Intercomparison Project Phase 6 (CMIP6) models

32 indicate ~~significant~~ great uncertainties in historical (1960–2014) global lightning trend simulations. Such uncertainties must be
33 investigated further.

34 **1 Introduction**

35 Lightning, an extremely energetic natural phenomenon, ~~always~~ occurs at every moment somewhere on Earth: its average
36 occurrence frequency is approximately 46 times per second (Cecil et al., 2014). Lightning generation is associated with electric
37 charge separation, which is mainly realized by collisions between graupel and hail and ~~other types of~~ hydrometeors of other
38 types within convective clouds (Lopez, 2016). As a natural ~~disaster~~ hazard, lightning can cause human and animal injuries
39 ~~or~~ and fatalities, infrastructure destruction, and wildfire ignition (Cerveny et al., 2017; Cooper and Holle, 2019; Jensen et al.,
40 2022; Veraverbeke et al., 2022). Lightning-produced NO_x (LNO_x) accounts for around 10% of the global tropospheric NO_x
41 (NO_x=NO+NO₂) source. It is regarded as the dominant NO_x source in the middle to upper troposphere (Schumann and
42 Huntrieser, 2007; Finney et al., 2016b). Moreover, LNO_x plays a ~~vital~~ crucially important role in atmospheric chemistry and
43 global climate by ~~controlling~~ affecting the abundances of OH radical, important greenhouse gases (GHGs) such as ozone and
44 methane, and other trace gases (Labrador et al., 2005; Schumann and Huntrieser, 2007; Wild, 2007; Liaskos et al., 2015;
45 Finney et al., 2016a; Murray, 2016; Tost, 2017; He et al., 2022b).

46
47 Reportedly, the lightning flash rate (LFR) is related to the stage of convective cloud development (Williams et al., 1989),
48 Convective Available Potential Energy (CAPE) (Romps et al., 2014), cloud liquid–ice water content (Saunders et al., 1991;
49 Finney et al., 2014), and even to the convective precipitation volume (Goodman et al., 1990; McCaul et al., 2009; Romps et
50 al., 2014). Long-term global warming is associated with changes in the overall temperature and relative humidity profiles in
51 the atmosphere and global convective adjustment (Manabe and Wetherald, 1975; Del Genio et al., 2007), which can strongly
52 affect the lightning-related factors described above. Consequently, long-term global warming can be a ~~crucially~~ fundamentally
53 important factor affecting long-term variations in global lightning activity. Findings from many earlier numerical simulation
54 studies manifest that global lightning activities are sensitive to long-term global warming, with most studies showing 5–16%
55 (average around 10%) increases in global lightning activities per 1 K global warming (Price and Rind, 1994; Zeng et al., 2008;
56 Hui and Hong, 2013; Banerjee et al., 2014; Krause et al., 2014; Romps et al., 2014; Clark et al., 2017). However, ~~minor~~ other
57 numerical simulation studies such as those using an ice-based lightning scheme or convective mass flux as a proxy to
58 parameterize lightning have yielded opposite results ~~(, suggesting that~~ global lightning activity will decrease under long-term
59 global warming) (Clark et al., 2017; Finney et al., 2018).

60
61 Aside from long-term global warming, changes in aerosol loading can also be responsible for long-term global lightning
62 activity variations. Aerosols influence lightning activity through aerosol radiative and microphysical effects, but the degree to
63 which the two distinct effects influence regional or global scale lightning activities remains unclear (Yuan et al., 2011; Yang

64 et al., 2013; Tan et al., 2016; Altaratz et al., 2017; Wang et al., 2018; Liu et al., 2020). Further research is needed. It is urgently
65 necessary to elucidate the effects of aerosol radiative and microphysical effects on lightning on a global scale. The aerosol
66 radiative effects indicate that aerosols can heat the atmospheric layer and can cool the Earth's surface by absorbing and
67 scattering solar radiation (Kaufman et al., 2002; Koren et al., 2004, 2008; Li et al., 2017). Thereby, convection and electrical
68 activities are likely to be inhibited (Koren et al., 2004; Yang et al., 2013; Tan et al., 2016). The microphysical effects suggest
69 that by acting as cloud condensation nuclei (CCN) or as ice nuclei, aerosols can reduce the mean size of cloud droplets,
70 ~~thereby consequently~~ suppressing the coalescence of cloud droplets into raindrops. ~~Consequently~~As a result, more liquid water
71 particles are uplifted to higher mixed-phase regions of the troposphere, where they invigorate lightning (Wang et al., 2018;
72 Liu et al., 2020).

73

74 The Earth has experienced ~~significant~~a considerable degree of global warming and changes in AeroPEs since the 1960s (Hoesly
75 et al., 2018; Climate at a Glance | National Centers for Environmental Information (NCEI), 2022). However, how historical
76 lightning has trended and how lightning has responded to historical global warming and changes in AeroPEs are not well
77 examined. This topic is worth exploring because historical lightning densities are indicators for all lightning-related phenomena
78 (Price and Rind, 1994). Exploring the historical global LNO_x emission trend is also meaningful because it can indicate the
79 effects of LNO_x emissions on atmospheric chemistry and global climate. Furthermore, investigating the effects of historical
80 global warming and increases in AeroPEs on historical lightning–LNO_x trends can provide a basis for assessing future
81 lightning–LNO_x trends.

82

83 Large-scale volcanic eruptions such as the 1991 Pinatubo eruption inject tremendous amounts of sulfuric gas into the
84 stratosphere, where it converts to H₂SO₄ aerosols. Consequently, the ~~size of the~~ stratospheric ~~aerosol layer is~~aerosols have
85 increased in abundance after the volcanic eruptions. The enhanced stratospheric aerosol layer can cool the Earth's surface
86 heterogeneously and can decrease the total amount of water in the atmosphere (Soden et al., 2002; Boucher, 2015, p.63). The
87 near-global perturbations in the radiative energy balance and meteorological fields caused by such strong volcanic eruptions
88 might influence global lightning activities. If so, there might be ramifications for all lightning-related phenomena. Nevertheless,
89 they remain poorly understood.

90

91 In our earlier work, we developed a new process and ice-based lightning scheme called the ECMWF-McCAUL scheme (He
92 et al., 2022b). This lightning scheme was developed by combining benefits of the lightning scheme used in the European
93 Centre for Medium-Range Weather Forecasts (ECMWF) forecasting system (Lopez, 2016) and those presented in reports by
94 ~~McCaul's work~~ et al. (McCaul et al., 2009). The ECMWF-McCAUL scheme simulated the best lightning density spatial
95 distributions among four existing lightning schemes when compared against satellite lightning observations (Lightning
96 Imaging Sensor (LIS) and Optical Transient Detector (OTD)) during 2007–2011. The sensitivity of global lightning activity

97 to changes in surface temperature on a decadal timescale ~~is was~~ estimated as 10.13% K⁻¹ ~~by using~~ the ECMWF-McCAUL
98 scheme (He et al., 2022b), which is close to most past estimates (average around 10% K⁻¹).

99

100 Using a chemistry–climate model CHASER (MIROC) with two lightning schemes (the widely used cloud top height scheme
101 and the ice-based ECMWF-McCAUL scheme), we ~~quantitatively~~ investigated historical lightning–LNO_x trends ~~quantitatively~~
102 and ~~found~~ ~~ascertained~~ how global warming, increases in AeroPEs, and ~~how~~ the Pinatubo eruption respectively influenced them.
103 Using two lightning schemes, we demonstrated the sensitivities of different lightning schemes to historical global warming,
104 increases in AeroPEs, and the Pinatubo eruption.

105

106 Research methods, including the model description and experiment setup, are described in Sect. 2. In Sect. 3.1, the simulated
107 historical lightning distributions and trends are validated ~~with using~~ LIS/OTD lightning observations. Section 3.2 presents the
108 effects of global warming and increases in AeroPEs on historical lightning–LNO_x trends. In Sect. 3.3, the ~~effects of the~~
109 Pinatubo volcanic eruption ~~effects~~ on historical lightning–LNO_x trends are discussed. Section 3.4 elucidated model
110 intercomparisons of ~~lightning flash rate~~ LFR trends and variation between our study (CHASER) and other CMIP6 model
111 outputs. Section 4 presents relevant discussions and conclusions ~~obtained from this~~ ~~based on these~~ study ~~findings~~.

112 2 Method

113 2.1 Chemistry–climate model

114 We used the CHASER (MIROC) global chemistry–climate model (Sudo et al., 2002; Sudo and Akimoto, 2007; Watanabe et
115 al., 2011; Ha et al., 2021) for this study, which incorporated consideration of detailed chemical and physical processes in the
116 troposphere and stratosphere. The CHASER version adopted for this study simulates the distributions of 94 chemical species
117 while reflecting the effects of 269 chemical reactions (58 photolytic, 190 kinetic, and 21 heterogeneous). As processes
118 associated with tropospheric chemistry, Non-Methane Hydrocarbons (NMHC) oxidation and the fundamental chemical cycle
119 of O_x–NO_x–HO_x–CH₄–CO are considered. CHASER simulates stratospheric chemistry involving the Chapman mechanisms
120 and catalytic reactions associated with HO_x, NO_x, ClO_x, and BrO_x. Moreover, it simulates the formation of polar stratospheric
121 clouds (PSCs) and ~~the~~ heterogeneous reactions occurring on their surfaces. CHASER is on-line-coupled to MIROC AGCM
122 ver. 5.0 (Watanabe et al., 2011), which simulates cumulus convection (Arakawa–Schubert scheme) and grid-scale large-scale
123 condensation to represent cloud and precipitation processes. The radiation flux is calculated using a two-stream k distribution
124 radiation scheme, which considers absorption, scattering, and emissions by aerosol and cloud particles as well as by gaseous
125 species (Sekiguchi and Nakajima, 2008; Goto et al., 2015). The aerosol component in CHASER is coupled with the
126 SPRINTARS aerosol model (Takemura et al., 2009), particularly for simulating primary organic carbon, sea-salt, and dust,
127 which is also based on MIROC. The aerosol radiation effects are considered in both large-scale condensation and cumulus
128 convection schemes, although the aerosol microphysical effects are only reflected in the large-scale condensation scheme.

130 This study used a horizontal resolution of T42 ($2.8^\circ \times 2.8^\circ$), with vertical resolution of 36 σ -p hybrid levels from the surface
 131 to approximately 50 km. Anthropogenic and biomass burning emissions were obtained from the CMIP6 forcing datasets (van
 132 Marle et al., 2017; Hoesly et al., 2018) for 1959–2014 (<https://esgf-node.llnl.gov/search/input4mips/>, last access: 19 September
 133 2022). Interannual variation in biogenic emissions for isoprene, monoterpene, acetone, and methanol₇ were considered using
 134 an off-line simulation by the Vegetation Integrative Simulator for Trace Gases (VISIT) terrestrial ecosystem model (Ito and
 135 Inatomi, 2012). The residual biogenic emissions (ethane, propane, ethylene, propene) used are climatological values derived
 136 from the Model of Emissions of Gases and Aerosols from Nature (MEGAN) modeling system (Guenther et al., 2012).

137

138 The CHASER (MIROC) global chemistry–climate model originally parameterizes lightning with the widely used cloud top
 139 height scheme (Price and Rind, 1992). A newly developed ice-based lightning scheme called the ECMWF-McCAUL here had
 140 been implemented into CHASER (MIROC) (He et al., 2022b). The ECMWF-McCAUL scheme computes **lightning flash**
 141 **rates LFRs** as a function of CAPE and ~~column precipitating ice (including Q_{Ra})~~ (Q_{Ra} represents the total volumetric amount of
 142 cloud ice, graupel, and snow **in the charge separation region**). Compared with the cloud top height, a salient advantage of the
 143 ECMWF-McCAUL scheme is that it has a direct physical link with the charging mechanism.

144 2.2 Lightning NO_x emission parameterizations

145 We tested two lightning schemes for this study. The first lightning scheme is the widely used cloud top height (CTH) scheme
 146 (Price and Rind, 1992), which was **used** originally ~~used~~ in CHASER (MIROC). This lightning scheme **calculates the lightning**
 147 **flash rate using** the following equations **to calculate LFR**.

$$148 F_l = 3.44 \times 10^{-5} H^{4.9} \quad (1)$$

$$149 F_o = 6.2 \times 10^{-4} H^{1.73} \quad (2)$$

150 Therein, F represents the total flash frequency (fl. min⁻¹), H stands for the cloud-top height (km), and subscripts l and o
 151 respectively denote the land and ocean (Price and Rind, 1992). Actually, we realize the CTH scheme in CHASER using the
 152 following equations (Eq. (3) and Eq. (4)). Each model layer's cumulus cloud fractions are used to weight the calculated
 153 lightning densities from that layer in the CTH scheme.

$$154 F_l = \sum_{i=1}^{n=36} adj_factor \times Cu_CF_i \times (H_i - H_{surface})^{4.9} \quad (3)$$

$$155 F_o = \sum_{i=1}^{n=36} adj_factor \times Cu_CF_i \times (H_i - H_{surface})^{1.73} \quad (4)$$

156 In those equations, i ~~denotes~~ **represents** the model layer index. ~~Also~~ **In addition**, adj_factor represents adjustment factors
 157 that differ for different model layers and model grids. Cu_CF_i symbolizes **the** cumulus cloud fraction at model layer i . H_i and
 158 $H_{surface}$ respectively denote the altitude of model layer i and the altitude of the model's surface layer.

159

160 The second lightning scheme used for this study is a newly developed one named the ECMWF-McCAUL scheme (He et al.,
 161 2022b), which is based on the original ECMWF scheme and findings reported by McCaul et al. (2009). The ECMWF-
 162 McCAUL scheme calculates lightning flash rates (LFRs) as a function of $CAPE$ ($m^2 s^{-2}$) and column precipitating ice (Q_{Ra})
 163 (Q_{Ra} symbolizes the total volumetric amount of cloud ice, graupel, and snow in the charge separation region) as

$$164 f_l = \alpha_l Q_{Ra} CAPE^{1.3} \quad (5)$$

$$165 f_o = \alpha_o Q_{Ra} CAPE^{1.3} \quad (6)$$

166 where f_l and f_o respectively symbolize the total flash density ($fl. m^{-2} s^{-1}$) over land and ocean. In addition, α_l and α_o are
 167 constants ($fl. s^{1.6} kg^{-1} m^{-2.6}$) determined after calibration against LIS/OTD climatology, respectively, for land and ocean. For
 168 this study, α_l and α_o are set respectively ~~to~~as 2.67×10^{-16} and 1.68×10^{-17} . In the charge separation region (from 0° to -
 169 $25^\circ C$ isotherm), Q_{Ra} ($kg m^{-2}$) is expressed as a proxy for the charging rate because of collisions between graupel and
 170 hydrometeors of other types (McCaul et al., 2009). Moreover, Q_{Ra} represents the total volumetric amount of
 171 precipitating hydrometeors of three kinds (graupel, snow, and cloud ice) within the charge separation region, calculated as

$$172 Q_{Ra} = \int_{z_0}^{z-25} (q_{graup} + q_{snow} + q_{ice}) \bar{\rho} dz, \quad (7)$$

173 where q_{graup} , q_{snow} , and q_{ice} respectively represent the mass mixing ratios ($kg kg^{-1}$) of graupel, snow, and cloud ice.

174 ~~Also~~In addition, q_{ice} was diagnosed using Arakawa–Schubert cumulus parameterization. Then, q_{graup} and q_{snow} were
 175 computed at each vertical level of the model using the following equations.

$$176 q_{graup} = \beta \frac{P_f}{\bar{\rho} V_{graup}} \quad (8)$$

$$177 q_{snow} = (1 - \beta) \frac{P_f}{\bar{\rho} V_{snow}} \quad (9)$$

178 In those equations, P_f represents the vertical profile of the frozen precipitation convective flux ($kg m^{-2} s^{-1}$), $\bar{\rho}$ denotes the air
 179 density ($kg m^{-3}$), and V_{graup} and V_{snow} respectively express the typical fall speeds for graupel and snow set to 3.1 and 0.5
 180 $m s^{-1}$ for this study. For land, the dimensionless coefficient β is set as 0.7, ~~while for oceans, whereas~~ it is set to 0.45; for oceans
 181 to consider the observed lower graupel content over the oceans.

182

183 Based on the cold cloud depth, a fourth-order polynomial (equation 10) is used to calculate the proportion of total flashes that
 184 are cloud-to-ground (p). An earlier report of the literature describes the method (Price and Rind, 1993).

$$185 p = \frac{1}{64.9 - 36.54D + 7.493D^2 - 0.648D^3 + 0.021D^4} \quad (10)$$

186 The depth of the cloud above the $0^\circ C$ isotherms is represented by D (km) in that equation.

187

188 According to recent studies, the intra-cloud (IC) lightning flashes are as efficient as cloud-to-ground (CG) lightning flashes
 189 at producing NO_x . The lightning NO_x production efficiency is estimated as 100–400 mol per flash (Ridley et al., 2005;
 190 Cooray et al., 2009; Ott et al., 2010; Allen et al., 2019). The LNO_x production ~~efficiency~~efficiencies for IC and CG are
 191 therefore set to the same value (250 mol per flash) in CHASER, which is the median of the commonly cited range of 100–

192 400 mol per flash. ~~Consequently~~Therefore, in this study, the distinctions between IC and CG do not affect the distribution or
193 magnitude of LNO_x emissions ~~in this study~~. It is noteworthy that marked uncertainties are involved in
194 ~~determining~~ascertaining the LNO_x production efficiency (Allen et al., 2019; Bucsela et al., 2019). The choice of a different
195 LNO_x production efficiency might affect the simulation of LNO_x emissions. Further research must be undertaken to
196 implement and validate a more sophisticated parameterization of LNO_x production efficiency in chemistry–climate models.
197 The calculated total column LNO_x for each grid was distributed into each model layer based on a prescribed “backward C-
198 shaped” LNO_x vertical profile (Ott et al., 2010).

199 **2.3 Lightning observation data for model evaluation**

200 We used LIS/OTD gridded climatology datasets for this study, consisting of climatologies of total ~~lightning flash rates~~LFRs
201 observed using the Lightning Imaging Sensor (LIS) and Optical Transient Detector (OTD). The OTD aboard the MicroLab-1
202 satellite and LIS aboard the Tropical Rainfall Measuring Mission (TRMM) satellite (Cecil et al., 2014). Both sensors
203 ~~detect~~detected lightning by monitoring pulses of illumination produced by lightning in the 777.4 nm atomic oxygen multiplet
204 above background levels. In low Earth orbit, both sensors ~~view~~viewed Earth locations for approximately 3 min during the pass
205 of the OTD or 1.5 min during passing of the LIS. ~~Each day~~, OTD and LIS ~~orbit~~respectively orbited the globe 14 times and 16
206 times ~~a day, respectively~~. OTD observed data between +75 and -75° latitude during May 1995 ~~through~~ March 2000, whereas
207 LIS collected data between +38 and -38° latitude during January 1998 ~~through~~ April 2015. This study uses the LIS/OTD 2.5
208 Degree Low Resolution Time Series (LRTS) ~~LRTS~~, which provides daily ~~lightning flash rates~~LFRs on a 2.5° regular latitude–
209 longitude grid for May 1995 ~~through~~ April 2015.

210 **2.4 CMIP6 model outputs for model comparison**

211 For the comparison of different model outputs from our study (CHASER) and other Earth system models or chemistry–climate
212 models, we used ~~the lightning flash rate~~LFR and surface temperature data from the CMIP6 CMIP Historical experiments from
213 CESM2-WACCM (Danabasoglu, 2019), GISS-E2-1-G (Kelley et al., 2020), and UKESM1-0-LL (Tang et al., 2019). CESM2-
214 WACCM uses the Community Earth System Model ver. 2 (Danabasoglu et al., 2020). The CESM2 is an open-source fully
215 coupled Earth system model. The Whole Atmosphere Community Climate Model ver. 6 (WACCM6) is the atmospheric
216 component coupled to the other components in CESM2. The GISS-E2-1-G is the NASA Goddard Institute for Space Studies
217 (GISS) chemistry–climate model version E2.1 based on the GISS Ocean v1 (G01) model (Miller et al., 2014; Kelley et al.,
218 2020). The UKESM1-0-LL is the UK's Earth system model, details of which ~~are~~were described by Sellar et al. (2019). We
219 used 3 ensembles from CESM2-WACCM, 9 ensembles from GISS-E2-1-G, and 18 ensembles from UKESM1-0-LL. Table
220 S1 presents all the ensemble members used for this study.

221 2.5 Experiment setup

222 We have conducted six sets of experiments with each set of experiments conducted using both the ECMWF-McCAUL
223 (abbreviated as F1) and CTH (abbreviated as F2) schemes. Table 1 presents the major settings of all experiments with the
224 relative explanations of those settings. STD-F1/F2 are standard experiments with the simulation period of 1959–2014. They
225 are aimed at reproducing intended to reproduce the historical trends of lightning and LNO_x. Climate1959-F1/F2 are experiments
226 that keep the climate simulations fixed to 1959 to derive the effects of global warming on historical lightning trends.
227 ClimateAero1959-F1/F2 are intended to reflect the conditions with climate simulations and aerosol and aerosol
228 precursorsprecursor (BC, OC, NO_x, SO₂) emissions fixed to 1959. The Aero1959-F1/F2 experiments are the same as the STD-
229 F1/F2 experiments, except for the AeroPEs fixed to 1959. The fifth set of experiments (Volca-off-F1/F2) was intended to
230 exclude the influences of the Pinatubo volcanic eruption to compare to the STD-F1/F2 and to evaluate the effects of the
231 Pinatubo eruption effects on historical lightning–LNO_x trends and variation.

232

233 We simulate volcanic aerosol forcing by considering the prescribed stratospheric aerosol extinction in the radiation scheme.
234 We used the NASA Goddard Institute for Space Studies (GISS) (Sato et al., 1993) and Chemistry–Climate Model Initiative
235 (CCMI) (Arfeuille et al., 2013) stratospheric aerosol dataset as the stratospheric aerosol climate data. The NASA GISS dataset
236 includes monthly zonal-mean stratospheric aerosol optical thickness in four spectral bands. The CCMI dataset for CHASER
237 includes monthly zonal-mean stratospheric aerosol extinction coefficients in 20 spectral bands. To remove the volcanic
238 perturbation but maintainwhile maintaining the stratospheric background aerosol in the Volca-off-F1/F2, we used the three-
239 sigma rulefollowing equation to process the Stratospheric Aerosol Climatology (SAC) during June 1991 – May 1994 using
240 the following equation. The three-sigma rule is often used to detect the outliers. This rule is appropriate to use here to discern
241 the outliers (the perturbation of SAC caused by a strong volcanic eruption).1996.

$$242 \quad SAC_{no_pinatubo} = \begin{cases} SAC_{background}, & |SAC_{raw} - SAC_{background}| > 3\sigma, \\ SAC_{raw}, & |SAC_{raw} - SAC_{background}| \leq 3\sigma \end{cases}$$
$$243 \quad \begin{cases} SAC_{background}, & |SAC_{raw} - SAC_{background}| > 1.96\sigma, \\ SAC_{raw}, & |SAC_{raw} - SAC_{background}| \leq 1.96\sigma \end{cases} \quad (11)$$

244 In that equation, $SAC_{no_pinatubo}$ denotes the stratospheric aerosol climatological data as input data for Volca-off-F1/F2
245 experiments, $SAC_{background}$ represents the stratospheric background aerosol climatological data (For this study,
246 $SAC_{background}$ is the corresponding temporal averaged values of the NSASNASA GISS and CCMI stratospheric aerosol
247 dataset during 2001–2010June 1986 – May 1991 and June 1996 – May 2001, when the time is close to the eruption and
248 the stratosphere was less affected by volcanic eruptions). SAC_{raw} stands for the original values of NSASNASA GISS
249 and CCMI stratospheric aerosol dataset during June 1991 – May 19941996. Moreover, σ symbolizes the standard
250 deviations of stratospheric background aerosol climate data (For this study, σ are the corresponding standard deviations

251 of ~~NSAS~~NASA GISS and CCMI stratospheric aerosol dataset during ~~2001–2010~~June 1986 – May 1991 and June 1996
252 – May 2001). As displayed in Eq. (11), when the absolute differences between SAC_{raw} and $SAC_{background}$ are larger
253 than 1.96σ , we replace the original values (June 1991 – May 1996) of the SAC with the temporal averaged values of the
254 NASA GISS and CCMI dataset during June 1986 – May 1991 and June 1996 – May 2001. When the absolute differences
255 between SAC_{raw} and $SAC_{background}$ are equal to or smaller than 1.96σ , we still use the original values (June 1991 –
256 May 1996) of the SAC for the Volca-off experiments. The value of 1.96σ corresponds to the 95% confidence interval,
257 which can remove the Pinatubo perturbation sufficiently but which can maintain the background level of stratospheric
258 aerosol during June 1991 – May 1996. Furthermore, the influences of the Pinatubo eruption ~~also~~ affected the HadISST
259 SSTs/sea ice fields. To remove the Pinatubo eruption's influences ~~in~~on the SSTs/sea ice fields ~~in~~from the Volca-off
260 experiments also, we ~~replae~~replaced the 1991-06 – 1995-05 SSTs/sea ice data with HadISST SSTs/sea ice climatological
261 data during 1985–1990 when conducting the Volca-off experiments. The 1985–1990 period was chosen because it is
262 ~~close to~~approximately the period of 1991-06 – 1995-05 and because the SSTs/sea ice fields were less affected by volcanic
263 activity during 1985–1990.

264

265 All the experiments calculate the LNO_x emissions rates interactively by LNO_x emission parameterizations except STD-
266 rVolcaoff experiments. The STD-rVolcaoff experiments are the same as the STD experiments except for reading the
267 daily LNO_x emission rates calculated from the Volca-off experiments. The STD-rVolcaoff experiments are conducted
268 for comparison with STD experiments to elucidate the effects of ~~the changed~~ LNO_x emissions changes caused by the
269 Pinatubo eruption on atmospheric chemistry (typically methane lifetime).

270

Table 1: All experiments conducted for this study

Name of experiment	Period	Climate (SSTs, sea ice, GHGs) ^a	Anthropogenic and biomass burning emissions	Biogenic emissions	Stratospheric aerosol climatology
STD-F1/F2 ^b	1959–2014	1959–2014	CMIP6 1959–2014		NASA GISS and CCMI stratospheric aerosol dataset ^c
Climate1959-F1/F2	1959–2014	Fixed to 1959 ^d	CMIP6 1959–2014	VISIT and MEGAN ^f	As above
ClimateAero1959-F1/F2	1959–2014	Fixed to 1959	AeroPEs fixed to 1959 ^e		As above
Aero1959-F1/F2	1959–2014	1959–2014	AeroPEs fixed to 1959		As above

Volca-off-F1/F2	1990– 1999	1990–1999 ^g	CMIP6 1990–1999	Same dataset with volcanic perturbation removed
STD-rVolcaoff- F1/F2	1990– 1999	All settings are the same as those used for STD experiment except for reading of the daily LNO _x emission rates calculated from the Volca-off experiments		

271 ^a For the model simulations, the climate is simulated by the prescribed SSTs/sea ice fields and the prescribed varying
272 concentrations of GHGs (CO₂, N₂O, methane, chlorofluorocarbons – CFCs – and hydrochlorofluorocarbons – HCFCs) used
273 only in the radiation scheme. The SSTs/sea ice fields are obtained from the HadISST dataset (Rayner et al., 2003). The
274 prescribed GHGs concentrations are derived from CMIP6 forcing datasets (Meinshausen et al., 2017).

275 ^b We use “F1” to stand for the ECMWF-McCAUL scheme; “F2” represents the CTH scheme.

276 ^c Stratospheric aerosol radiative forcing is simulated using the prescribed stratospheric aerosol extinction, which is obtained
277 from the NASA GISS (Sato et al., 1993) and CCM1 (Arfeuille et al., 2013) stratospheric aerosol dataset.

278 ^d The climate is fixed to 1959 for the whole simulation period using the 1959 SSTs/sea ice field and GHG concentrations
279 during the simulation period.

280 ^e Aerosol (BC, OC) and aerosol ~~precursors~~precursor (NO_x, SO₂) emissions (anthropogenic + biomass burning) are fixed to
281 1959 throughout the simulation period.

282 ^f Several biogenic emissions are interannually varying, including isoprene, monoterpenes, acetone, and methanol, which were
283 calculated using an off-line simulation ~~by using~~ the Vegetation Integrative Simulator for Trace Gases (VISIT) terrestrial
284 ecosystem model (Ito and Inatomi, 2012). Some other reactive biogenic VOCs (ethane, propane, ethylene, propene) used are
285 climatological data derived from the Model of Emissions of Gases and Aerosols from Nature (MEGAN) modeling system
286 (Guenther et al., 2012).

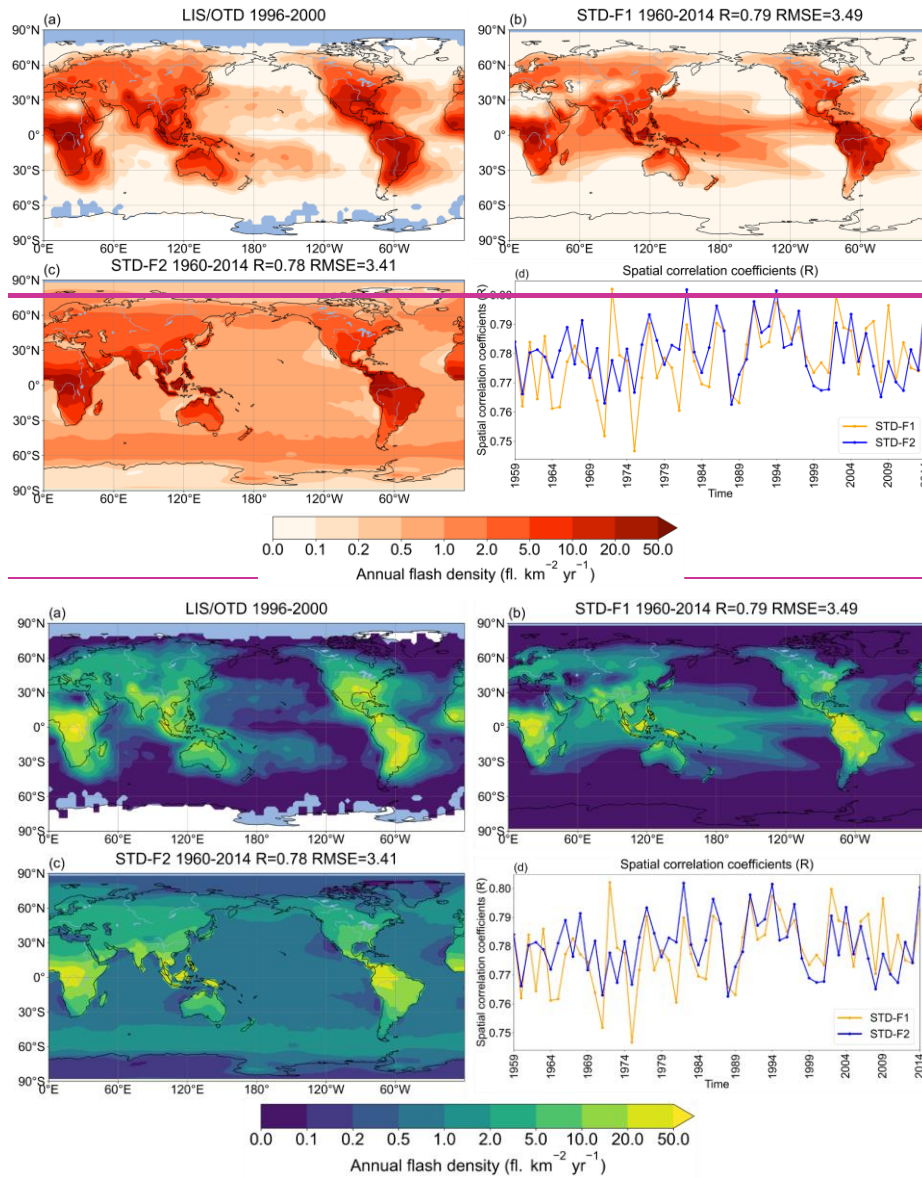
287 ^g Here the 1991-06 – 1995-05 SSTs/sea ice data were replaced with HadISST SSTs/sea ice climatological data during
288 1985–1990.

289 **3 Results and Discussion**

290 **3.1 Validation of the simulated historical lightning distribution and trend**

291 To increase the credibility of the conclusions obtained based only on the numerical simulations, the model calculations must
292 be evaluated using observational data. We used the LIS/OTD observations to evaluate the spatial ~~and temporal~~ distribution
293 and historical lightning trends simulated by CHASER (MIROC). Figures 1a–~~e1c~~ show the annual mean spatial
294 ~~distribution~~distributions of lightning observed by LIS/OTD and from model simulations using the ECMWF-McCAUL and
295 CTH schemes. Both the ECMWF-McCAUL and CTH schemes generally captured the hotspots of lightning (Central Africa,
296 Maritime Continent, South America), with strong spatial correlations between observations and model simulations ($R > 0.75$).

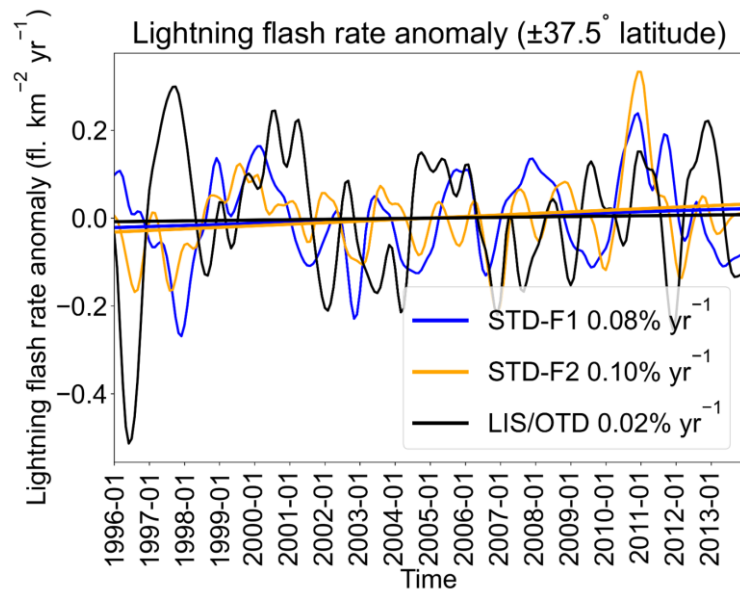
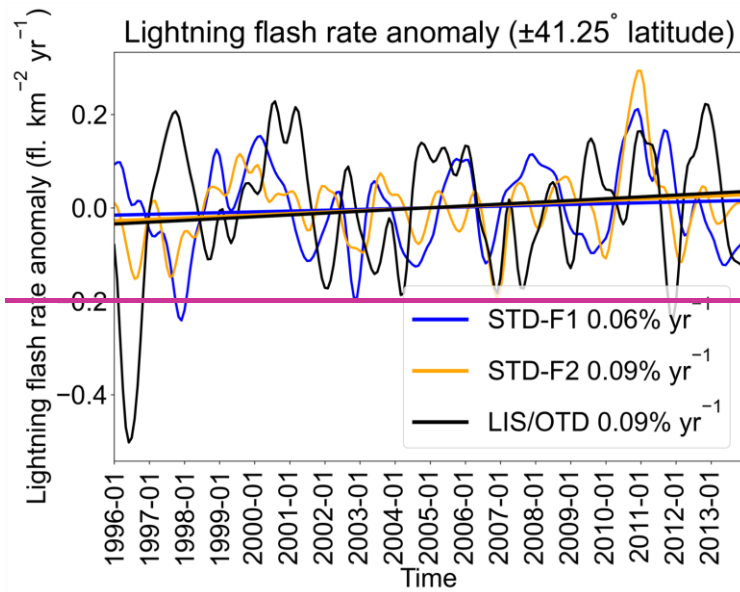
297 Figure 1d exhibits strong spatial correlation between observations and simulation results maintained throughout the simulation
 298 period (1959–2014).



299

300

301 Figure 1: Annual mean lightning flash densities from (a) LIS/OTD satellite observations spanning 1996–2000, (b) the STD
 302 experiment (1960–2014) with the ECMWF-McCAUL scheme used, (c) the STD experiment (1960–2014) with the CTH scheme used.
 303 R and RMSE shown in the titles of panels (b) and (c) are calculated between panels (b)-(c) and (a). Panel (d) presents the spatial
 304 correlation coefficients between modeled annual mean spatial lightning densities distribution of each year and LIS/OTD lightning
 305 climatologies during 1996–2000.



306

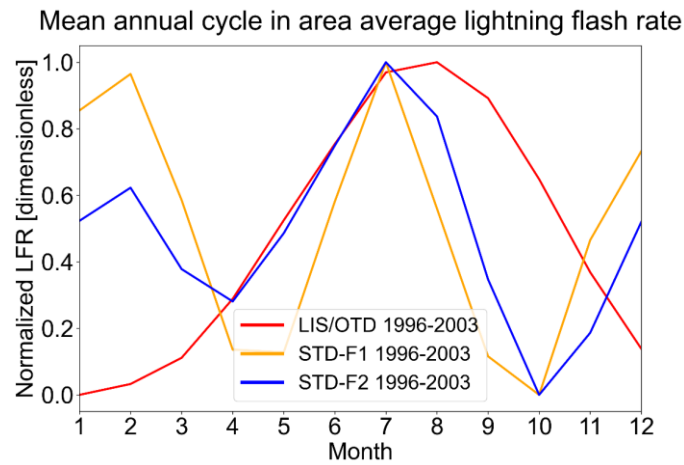
307

308 **Figure 2: Lightning flash rate**LFR anomalies of 1996–2013 within ± 41.25 37.5 $^{\circ}$ latitude obtained from two numerical experiments
 309 (STD-F1 **and** STD-F2) and LIS/OTD satellite observations. Curves represent the monthly time-series data of the ± 41.25 37.5 $^{\circ}$
 310 latitude mean **lightning flash rate**LFR anomalies with the 1-D Gaussian (Denoising) filter applied. Lines are the fitting curves of the
 311 monthly time-series data of the ± 41.25 37.5 $^{\circ}$ latitude mean **lightning flash rate**LFR anomalies. Trends of the **lightning flash rate**LFR
 312 anomalies in % yr⁻¹ are also **shown**presented in the legends.

313

314 The LIS/OTD observations are also used to evaluate historical lightning trends simulated by CHASER (MIROC). **Because**
 315 **almost all valid LIS/OTD observations exist only within $\pm 41.25^{\circ}$ latitude during 1996–2013,** We examined the ± 41.25 37.5 $^{\circ}$

316 latitude mean lightning flash rateLFR anomaly (1996–2013) calculated from LIS/OTD observations and STD-F1/F2 numerical
 317 experiments (Fig. 2). We also note some missing values within the $\pm 41.2537.5^\circ$ latitude in LIS/OTD observations. To
 318 keep constrain the comparisons between observations and simulations as like-for-like, when we encounter a missing value in
 319 the LIS/OTD observations during spatial averaging, we also treat the CHASER simulated value at the same location as a
 320 missing value. As displayed in Fig. 2, even when the interannual variations of the lightning flash rateLFR anomaly sometimes
 321 differ between observations and simulations, the overall trends of lightning flash rateLFR anomaly simulated by using both
 322 schemes well matched the LIS/OTD observations. Neither the lightning flash rateLFR anomaly (within $\pm 41.2537.5^\circ$ latitude)
 323 derived from LIS/OTD observations nor simulations show a significant trend for 1996–2013 using the Mann–Kendall rank
 324 statistic test (significance set as inferred for 5%). The global lightning flash rateLFR anomaly (during 1993–2013) obtained
 325 from simulations (STD-F1/F2) also show shows no significant trend, which is consistent with the Schuman Resonance (SR)
 326 intensity observations (1993–2013) at Rhode Island, USA (Earle Williams, 2022). However, the SR observations in Rhode
 327 Island (USA) exclude consideration of the influences of solar cycles, which makes it less appropriate for lightning trend
 328 evaluation.



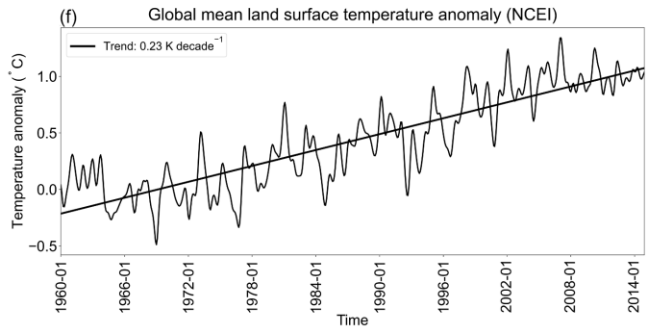
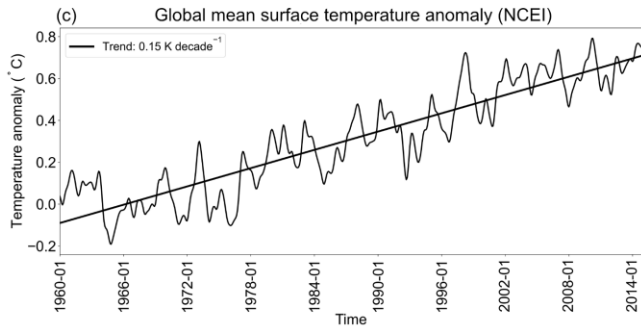
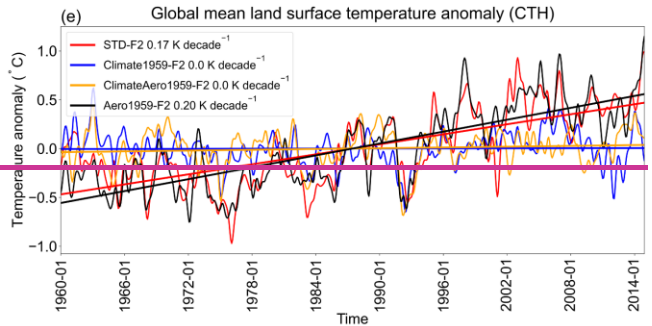
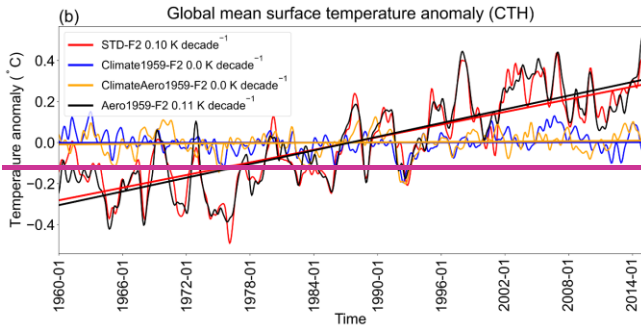
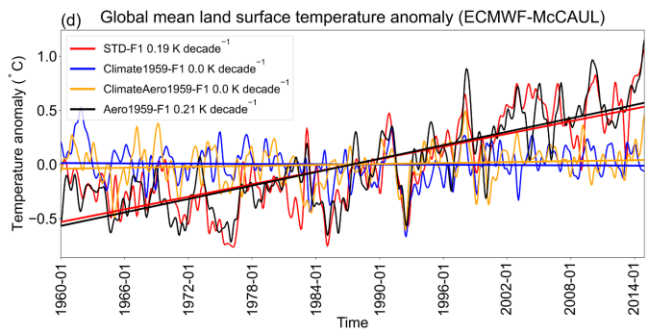
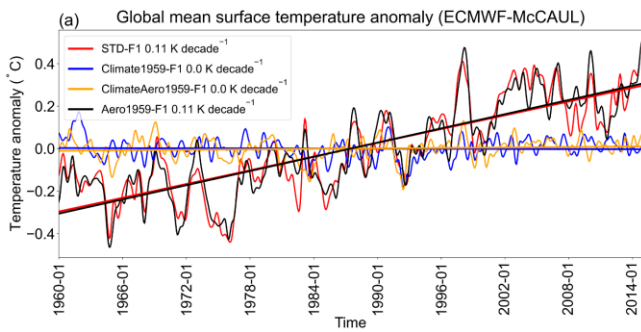
329
 330 **Figure 3: Mean annual cycle in area average LFR during 1996–2003. The area average was taken over the grid cells where valid**
 331 **LIS/OTD lightning observations exist. LFR is normalized by min-max normalization.**

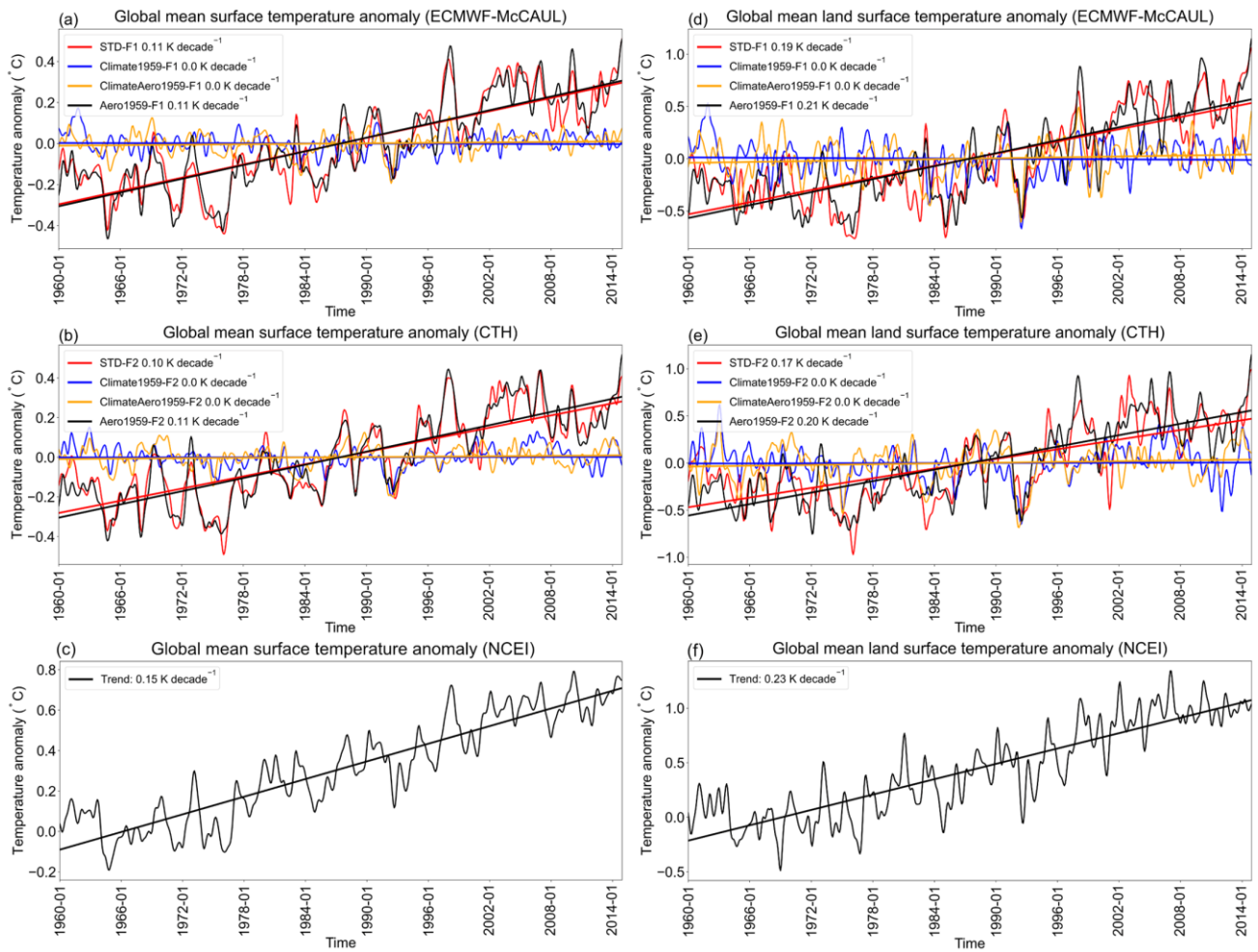
332
 333 We further investigated the seasonal variabilities of simulated LFR and compared them against LIS/OTD observations. The
 334 results are depicted in Fig. 3. Both the CTH and ECMWF-McCAUL schemes captured the peak during JJA, but the
 335 overestimation of LFR by F1/F2 during DJF is also noticeable. Figure S1 presents comparison of the LFR global distribution
 336 in different seasons during 1996–2003 from LIS/OTD lightning observations and STD experiment outputs. Generally,
 337 CHASER well-captured the spatial distribution of LFR in all four seasons when compared against LIS/OTD observations. The
 338 spatial correlation coefficients (R) between observations and simulations are highest (R=0.80 for both lightning schemes) in
 339 DJF, indicating CHASER’s considerable capability to reproduce the LFR spatial distribution in DJF. As displayed in the first
 340 row of Fig. S1, the overestimation of LFR by F1/F2 during DJF is primarily attributable to the overestimation of LFR within

341 the Maritime Continent and South America, but this might also be attributable to the underestimation of LFR by LIS/OTD
342 within these two regions. It is believed that the LIS/OTD lightning detection efficiency is highly sensitive to the characteristic
343 of convective clouds (cloud albedo, cloud optical thickness, etc.) (Boccippio et al., 2002; Cecil et al., 2014). High cloud albedo
344 and cloud optical thickness might engender the underestimation of LFR by LIS/OTD. It is also noteworthy that the seasonal
345 variation and long-term trend of global lightning are strongly influenced by distinct different factors. The seasonal variation
346 of global lightning activities is most strongly affected by the 23° obliquity of Earth’s orbit and the asymmetric distribution of
347 the continent between the Northern and Southern hemispheres. However, the long-term global lightning trend we investigated
348 for this study is controlled mainly by climate forcings such as aerosols and GHGs. To minimize the effects of LFR seasonal
349 variation on our study’s results, we deseasonalized the results shown in all figures and tables by calculating their anomaly
350 based on raw data. The validation described above and the deseasonalization of our study’s results justified that the LFR
351 seasonal variation (and the uncertainties in the simulation of LFR seasonal variation) in our study has a limited effect on these
352 study results.

353 **3.2 Effects of global warming and increases in AeroPEs on historical lightning–LNO_x trends**

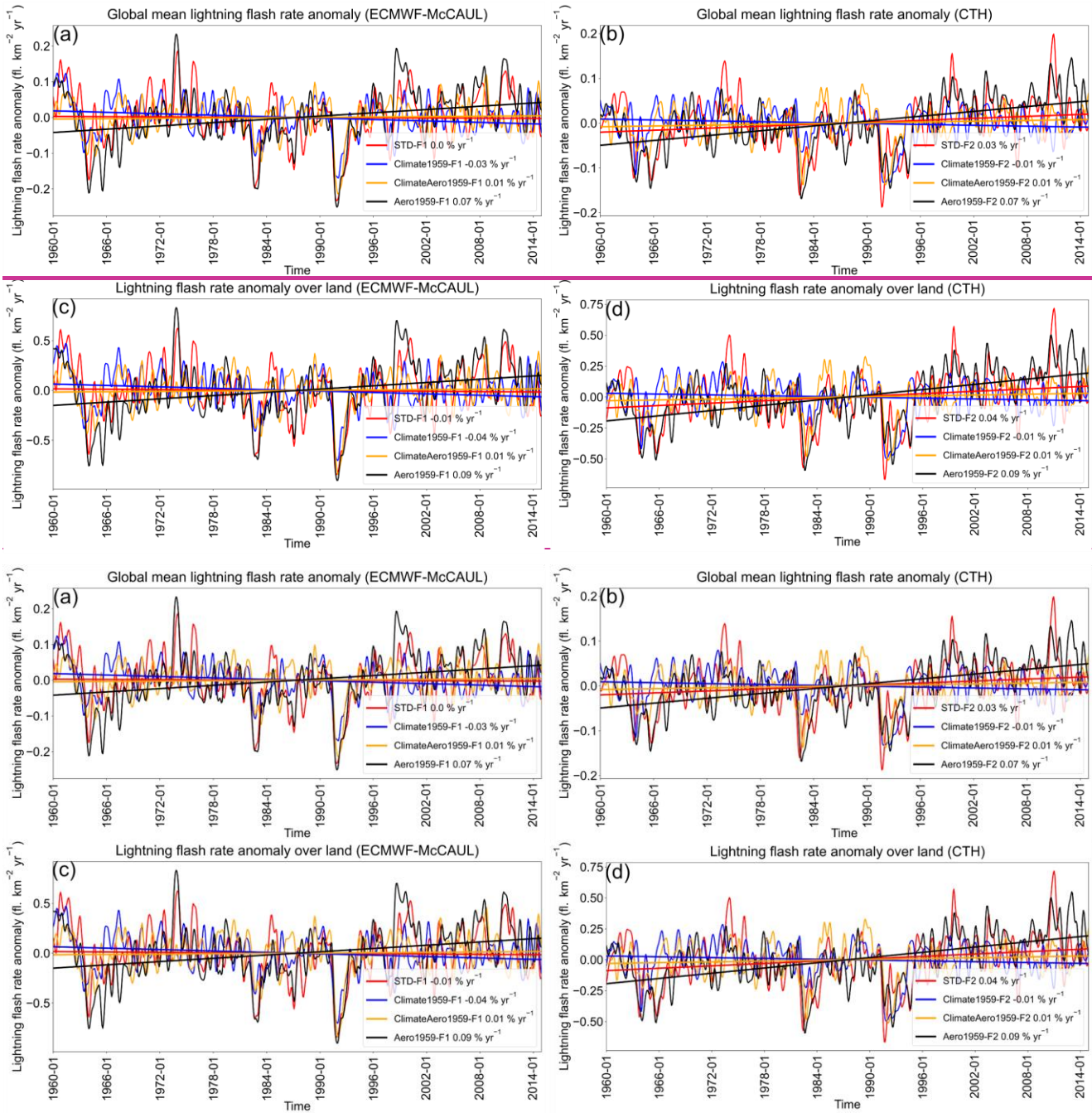
354 As introduced in Sect. 1, global warming and changes in AeroPEs are the two main factors which influence ~~the~~ long-term
355 (1960–2014) historical lightning trends (Hereinafter, historical lightning trends ~~indicate~~represent lightning trends of 1960–
356 2014.). To analyze the effects of global warming on historical lightning trends, we designed and conducted two sets of
357 experiments: one set of experiments including “global warming” (STD-F1/F2) and another set of experiments excluding
358 “global warming” (Climate1959-F1/F2). Figures ~~3a4a~~ and ~~3b4b~~ respectively depict the global surface temperature anomalies
359 calculated ~~from~~using the ECMWF-McCAUL and CTH schemes. The STD and Aero1959 experiments show an increasing
360 trend (around 0.11 K decade⁻¹) of global mean surface temperature anomalies, which ~~is close to~~closely approximates the trend
361 (around 0.15 K decade⁻¹) obtained from NOAA’s National Centers for Environmental Information (NCEI) (Figs. 4c, 4f).
362 Global temperature change data from 1880 to the present are available from the NCEI, which tracks ~~the~~ variations of the
363 Earth’s temperature based on thousands of stations’ observation data around the globe (Climate at a Glance | National Centers
364 for Environmental Information (NCEI), 2022). When the prescribed SSTs/sea ice fields and GHGs concentrations were fixed
365 to 1959 throughout the simulation period, the simulated trends of global mean surface temperature anomalies turned out to be
366 flat (Climate1959 and ClimateAero1959). To elucidate the effects of increases in AeroPEs on averaged surface temperature to
367 the greatest extent possible, we also show the averaged surface temperature anomaly only over land regions (Figs. ~~3d–f4d–4f~~).
368 The simulated global mean land surface temperature anomalies are also well-matched with the NCEI observational data. The
369 aerosol cooling effect can be more evident when only ~~particularly addressing~~examining surface temperature trends averaged
370 over land (Figs. ~~3d–e4d–4e~~).





372

373 **Figure 34:** Monthly time-series data of global mean surface temperature anomalies with 1-D Gaussian (Denosing) filter applied and
 374 their fitting curves calculated from the outputs of numerical experiments (a–b) and obtained from NCEI (c). **Figures 3d–Panels (d)–**
 375 **(f)** are the same as **Figs. 3a–panels (a)–(c)**, but the averaged surface temperature anomalies are only calculated within the global
 376 land regions. The trends of the fitting curves in K decade⁻¹ are also presented in the legends.



377

378

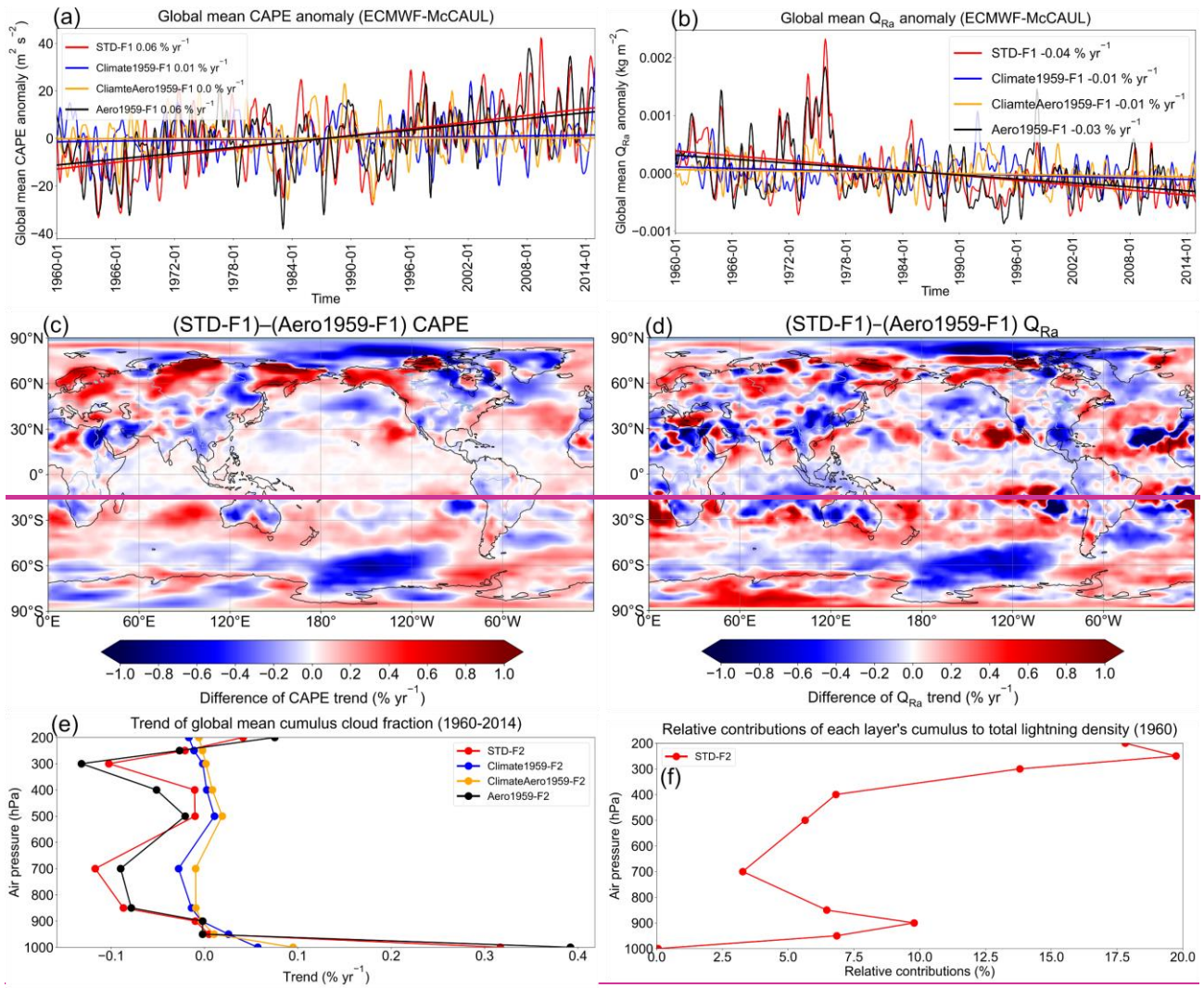
379 **Figure 4: Figures 45: Panels (a) and (b) show monthly time-series data of global mean lightning flash rate LFR anomalies with 1-D**
 380 **Gaussian (Denoising) Filter applied and their fitting curves of different experiments simulated respectively using the ECMWF-**
 381 **McCAUL scheme and CTH scheme. Figures 4panels (c) and (d) are the same as Figs. 4panels (a) and (b), except that the averaged**
 382 **lightning flash rate LFR anomalies are calculated only within global land regions. Trends of the fitting curves (% yr⁻¹) are also shown**
 383 **in the legends.**

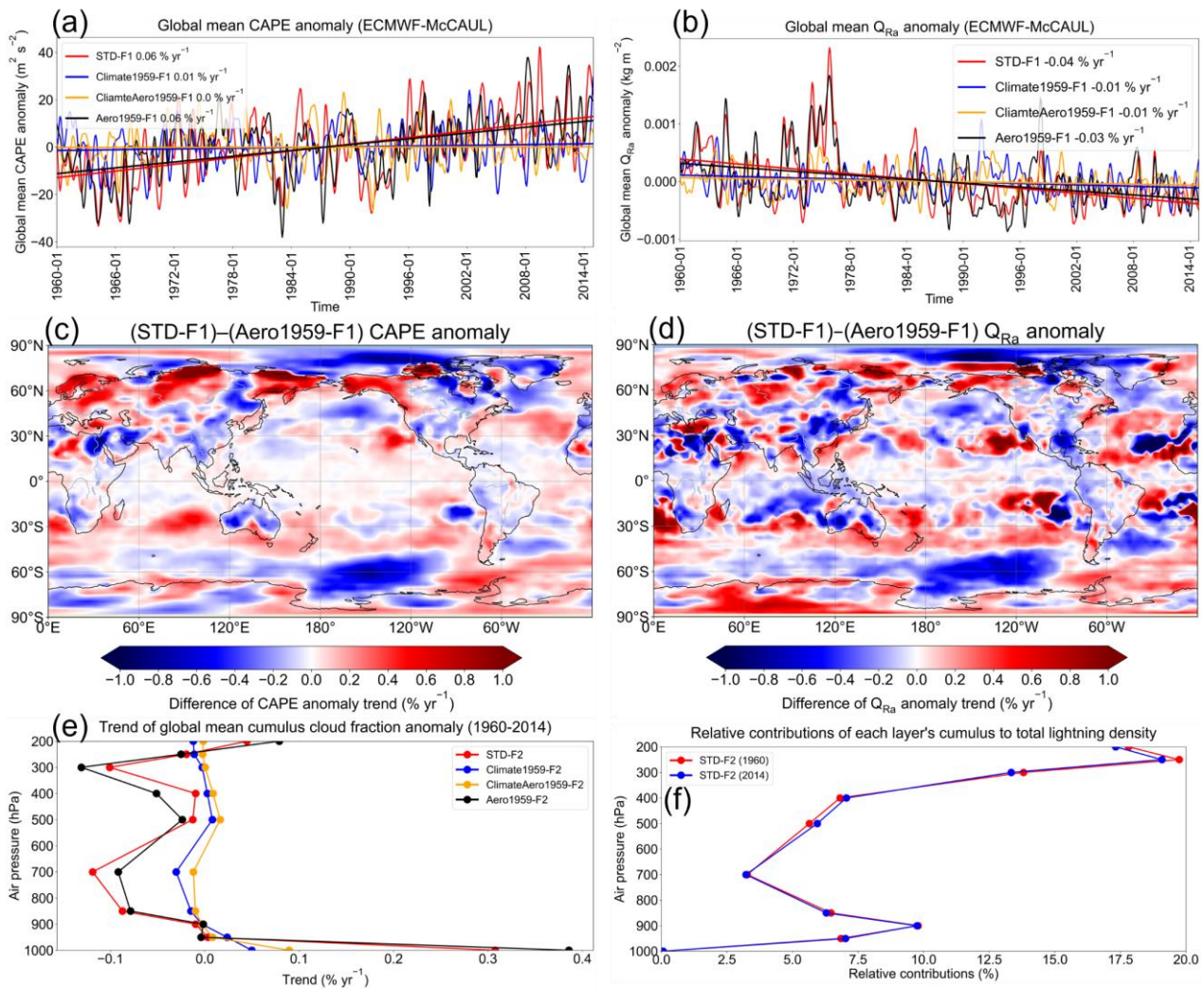
384

385 ~~Figures 4~~Figure 5. panels (a) and (b) respectively ~~show~~portray the global mean ~~lightning flash rate~~LFR anomalies and their
386 fitting curves obtained from the outputs of the ECMWF-McCAUL scheme and CTH scheme. The global lightning trend
387 obtained from the STD-F1 experiment turned out to be statistically flat ($0.0\% \text{ yr}^{-1}$), whereas the outputs of the STD-F2
388 experiment exhibit a not significant increasing global lightning trend ($0.03\% \text{ yr}^{-1}$) determined using the Mann–Kendall rank
389 statistic (significance inferred for 5%).

390

391 ~~From~~ Comparison of the lightning trends calculated from the STD and Climate1959 experiments, ~~we found~~ showed that both
392 lightning schemes demonstrated that ~~the~~ historical global warming (1960–2014) enhances the global lightning trends toward
393 positive trends (around $0.03\% \text{ yr}^{-1}$ or $3\% \text{ K}^{-1}$). ~~The effects of~~ Global warming ~~effects~~ on historical lightning trends ~~are~~ were
394 evaluated as significant using the Mann–Kendall rank statistic, with significance inferred for 5%. when using the CTH scheme,
395 but not in the case of the ECMWF-McCAUL scheme (Hussain and Mahmud, 2019). The differences in lightning trends
396 simulated by the STD-F1/F2 and Aero1959-F1/F2 experiments indicate that the increases in AeroPEs during 1960–2014
397 significantly suppress the global lightning trends ($-0.07\% \text{ yr}^{-1}$ – $-0.04\% \text{ yr}^{-1}$). It is noteworthy that this suppression of lightning
398 trends is only attributable to ~~the~~ aerosol radiative effects. Further research ~~is needed~~ must be conducted to elucidate the long-
399 term effects of ~~aerosol~~ aerosols on lightning through aerosol microphysical effects. We also investigated lightning trends only
400 over land regions (Figs. ~~4e–4~~ 5c–5d) to ascertain the effects of changes in AeroPEs to the greatest extent possible. When
401 observing the lightning trends over land only, the degree of suppression of lightning trends ~~by~~ attributable to increases in
402 AeroPEs expands to $-0.10\% \text{ yr}^{-1}$ – $-0.05\% \text{ yr}^{-1}$, which is attributable to most AeroPEs and their growth coming from land
403 regions. It is noteworthy that we used the same SSTs/sea ice data in the Aero1959 as those used for STD experiments. The
404 SSTs/sea ice data also reflected the effects of increases in AeroPEs. Therefore, we might underestimate the effects of increases
405 in AeroPEs on lightning trends by comparing the results of STD and Aero1959 experiments.





407

408 **Figure 5: Figures 5a-f:** Panels (a) and (b) respectively show monthly time-series data of global mean CAPE and Q_{Ra} anomalies with
 409 1-D Gaussian (Denoising) filter applied and their fitting curves simulated using the ECMWF-McCAUL scheme. **Figure 5c** Panels (c)
 410 and (d) respectively show differences in the CAPE anomaly trend and Q_{Ra} anomaly trend of the STD-F1 and Aero1959-F1
 411 experiments in the global map. **Figure 5e** Panel (e) portrays the vertical profiles of the trend of global mean cumulus cloud fraction
 412 trend anomaly simulated by the CTH scheme. **Figure 5f** Panel (f) depicts the relative contributions of each layer's cumulus to total
 413 lightning density in 1960 and 2014, as calculated from the outputs of the STD-F2 experiment.

414

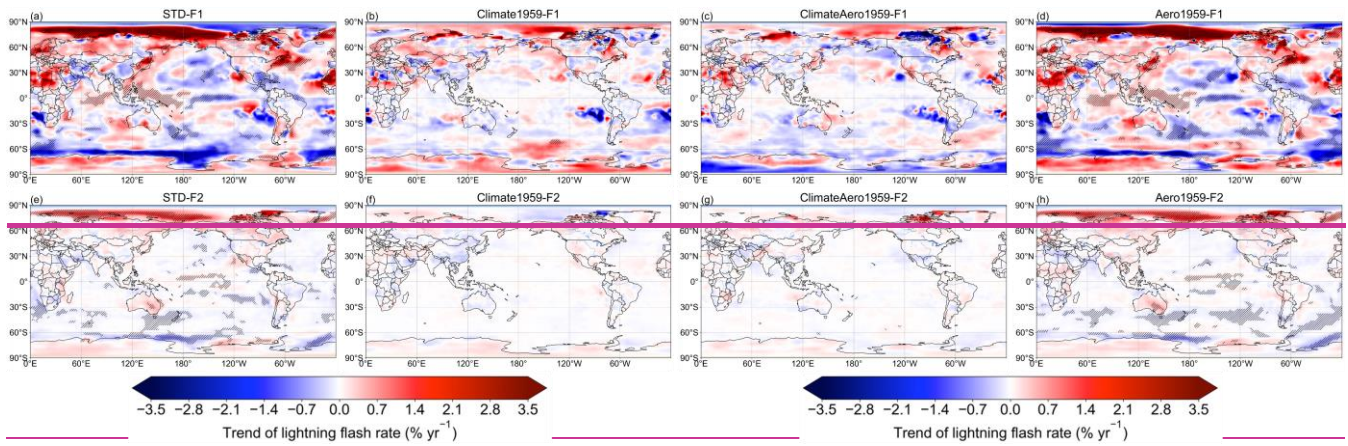
415 For the ECMWF-McCAUL scheme, model outputs affirm that global warming can enhance the global mean CAPE anomaly
 416 slightly and suppress the global mean Q_{Ra} anomaly (Figs. 5a–5b). Earlier studies have also indicated that the total solid (cloud
 417 ice, snow, and graupel) mass mixing ratio within charge separation regions is lower under global warming. Moreover, possible
 418 explanations are given in those studies (Finney et al., 2018; Romps, 2019) 5a–b). The trend of the global mean Q_{Ra} anomaly

419 ~~can be suppressed by earlier global warming, probably because global warming engenders the shifting of the 0°C—25°C~~
420 ~~isotherm to the higher region.~~ Because global warming enhances global convection activities, and because lightning formation
421 is highly related to convection activity, global warming enhances the historical global lightning trend simulated ~~by using~~
422 ECMWF-McCAUL scheme, mainly as a result of the simulated CAPE trend, which is enhanced by global warming. The past
423 increases in AeroPEs exert negligible effects on the trends of global mean CAPE and Q_{Ra} anomalies, as displayed in Figs. ~~5a–~~
424 ~~6a–6b~~. However, the past increases in AeroPEs suppress the CAPE and Q_{Ra} trend within the tropical and subtropical terrestrial
425 regions, where lightning densities are high (Figs. ~~5e–6c–6d~~). Weaker convection activities (smaller CAPE) and fewer
426 hydrometeors (cloud ice, graupel, snow) in the charge separation regions (0°C – -25°C isotherm) ~~lead to engender~~ less lightning.
427 These are the main causes for the suppression of the historical lightning trends induced by increases in AeroPEs through
428 aerosol radiative effects. ~~It is noteworthy that, because the aerosol microphysical effects are only considered in the grid-scale~~
429 ~~large-scale condensation scheme, our study might underestimate the aerosol microphysical effects which can enhance the~~
430 ~~trends of Q_{Ra} and LFR toward the positive direction.~~

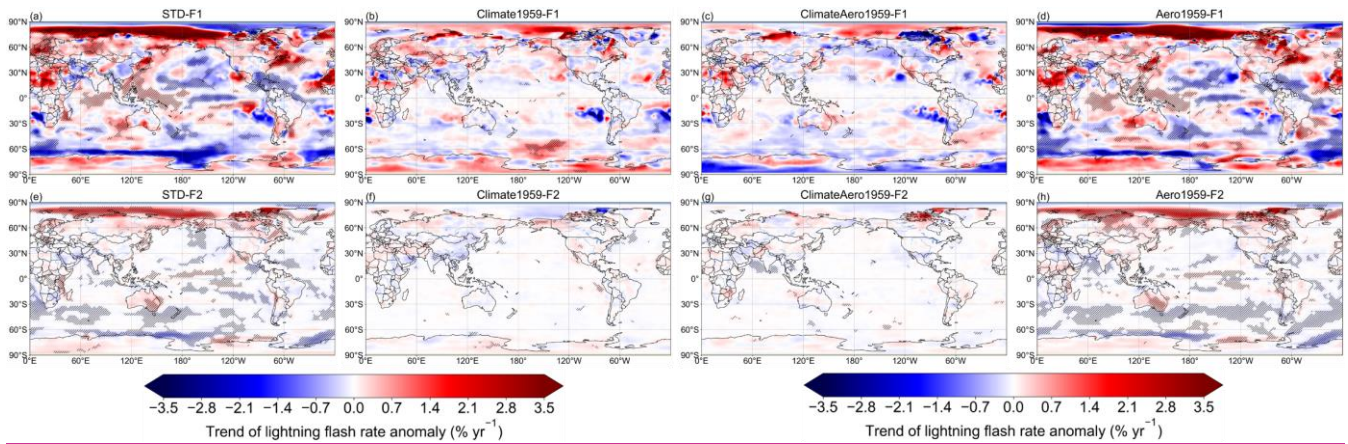
431

432 To explain the results simulated by the CTH scheme, we investigated the vertical profiles of the trend of the global mean
433 cumulus cloud fraction (~~Fig. 5e~~). ~~This anomaly (Fig. 6e). Investigating cumulus cloud fraction~~ is reasonable because each
434 model layer's cumulus cloud fractions are used to weight the calculated lightning densities from that layer in the CTH scheme,
435 as introduced in equations (3) and (4). Figure ~~5f6f~~ shows the relative contributions of each model layer's cumulus to the
436 calculated global total lightning densities in 1960 ~~by the CTH scheme and 2014 obtained using the CTH scheme. As Fig. 6f~~
437 ~~displayed, the vertical profiles of relative contribution in 1960 and 2014 are almost identical.~~ Cumulus convection is positively
438 correlated with lightning formation, which is the scientific basis of parameterizing lightning densities using the cumulus cloud
439 top height: the CTH scheme. ~~The~~ Historical global warming enhances the lightning trend simulated by the CTH scheme mainly
440 because the simulated historical global warming increases the cumulus reaching 200 hPa, which ~~contribute~~ ~~contributes~~ greatly
441 to the simulated global total lightning density (Figs. ~~5e–6e–6f~~). The increases in the deep convective cloud are regarded as
442 related to the increases in tropopause height attributable to global warming, ~~which is as~~ shown in Fig. ~~S1S2~~. The past increases
443 in AeroPEs suppress the lightning trend simulated by the CTH scheme because increases in AeroPEs decrease the cumulus
444 reaching 200 hPa as well as the cumulus within the lower to middle troposphere ~~by aerosol radiative effects (Fig. 5f). Also 6e~~.
445 ~~In addition~~, in the supplement, we present a figure (Fig. ~~S2S3~~) resembling Fig. ~~56~~, but which includes only consideration of
446 land regions. The mechanisms of global warming and increases in AeroPEs affecting lightning trends over land regions are
447 similar to those described above on a global scale. We do not discuss ~~details of them in detail~~ here.

448

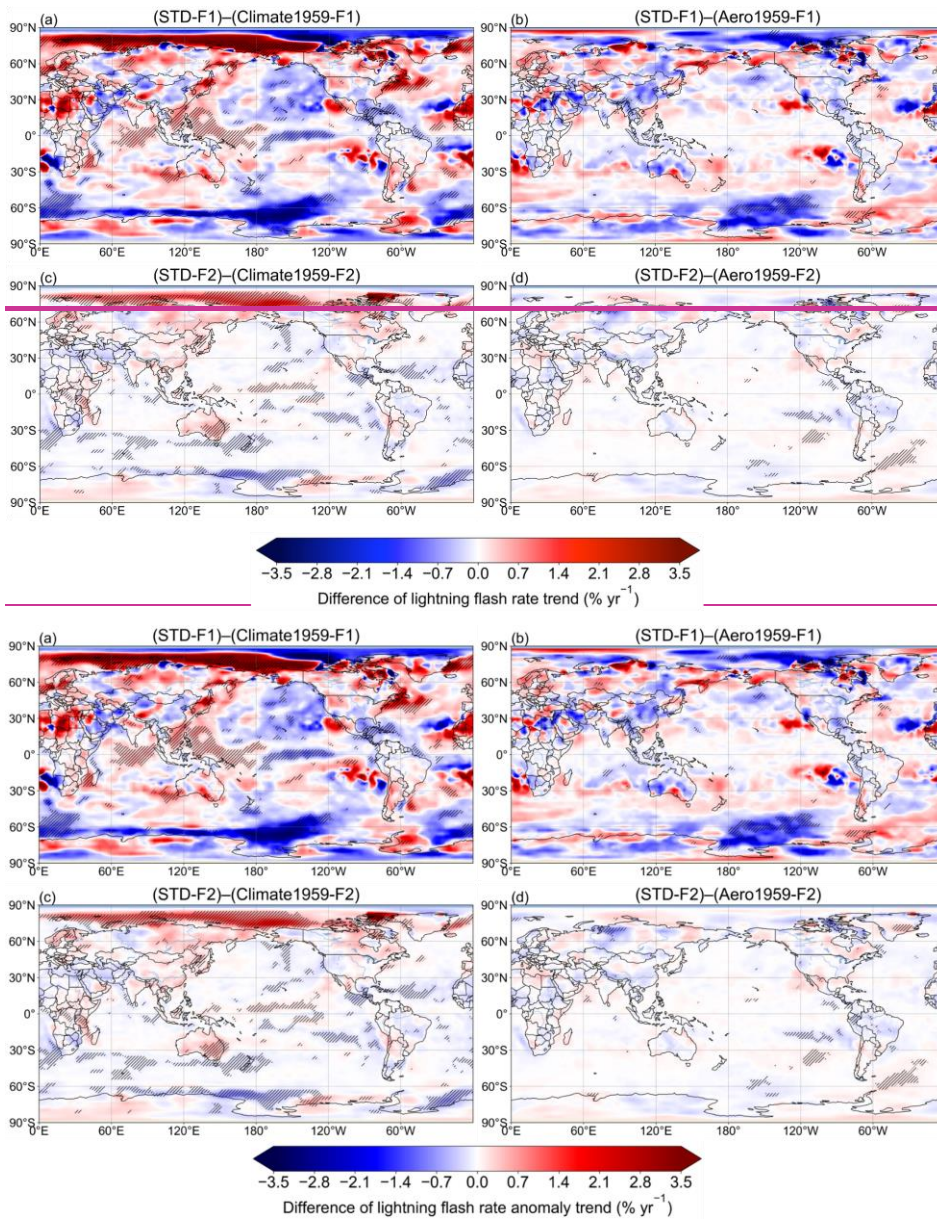


449



450

451 **Figure 6: Lightning flash rate trends**
 452 **7: Trends of LFR anomaly ($\% \text{ yr}^{-1}$) during 1960–2014 on the two-dimensional map. The trend**
 453 **at every point was calculated from the function of approximating curve for the 1960–2014 time-series data (LFR anomaly)**
 454 **at each grid cell. The area in which the trend was found to be significant by the Mann–Kendall rank statistic test (significance level**
 455 **inferred for 5%) is marked with hatched lines.**



456

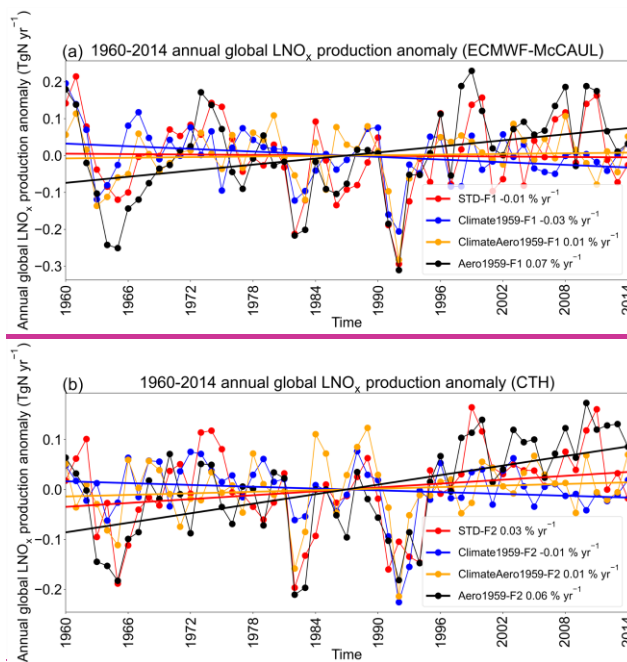
457

458 **Figure 78:** Differences in lightning flash rate trends of LFR anomaly during 1960–2014 on the global map. The area in which the
 459 trend of the differences of lightning flash rate LFR anomaly time-series data was found to be significant by the Mann–Kendall rank
 460 statistic test (significance level inferred for 5%) is marked with hatched lines.

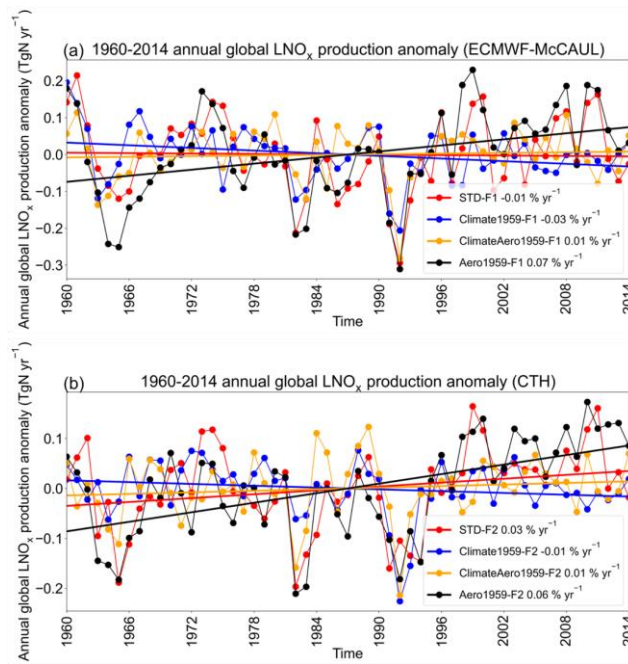
461

462 We also investigated lightning trends simulated from different experiments with the global map (Fig. 67). Both the ECMWF-
 463 McCAUL and the CTH schemes show that the lightning increased significantly in most parts of the Arctic region and decreased
 464 in some parts of the Southern Ocean during 1960–2014 (Figs. 6a, e7a, 7e). The significant lightning trends presented in Figs.

465 6a almost disappeared 7a became nearly nonexistent when the climate simulations were fixed to 1959 (Figs. 6b, f7b, 7f),
 466 indicating the considerable effects of global warming on the trend of global lightning activities. Furthermore, the effects of
 467 past global warming and increases in AeroPEs on the lightning trends on the global map are displayed in Fig. 78. Figures 7a,
 468 e indicate 8a and 8c show that past global warming enhances lightning activities within the Arctic region and Japan, which is
 469 consistent with findings of an earlier study from which Japan thunder day data were reported (Fujibe, 2017). Figures 7a, e 8a
 470 and 8c also show that historical global warming suppresses lightning activities around New Zealand and some parts of the
 471 Southern Ocean. Both lightning schemes demonstrated that the historical increases in AeroPEs suppress lightning activities in
 472 some parts of the Southern Ocean and South America. The ECMWF-McCAUL scheme also suggests that historical increases
 473 in AeroPEs suppress lightning activities by aerosol radiative effects in some parts of India and China, where AeroPEs increased
 474 dramatically during 1960–2014 because of rapid economic development and energy consumption. Many observation-based
 475 studies indicate that aerosols can invigorate lightning activities in some regions of China and India, typically under relatively
 476 clean conditions (e.g., AOD < 1.0), which is attributable to the aerosol microphysical effects (Wang et al., 2011; Zhao et al.,
 477 2017; Lal et al., 2018; Liu et al., 2020; Shi et al., 2020; Zhao et al., 2020). Therefore, a total positive effect of aerosol on
 478 historical lightning trends in China and India cannot be ruled out. We further provided the same figures as Figs. 67 and 78, but
 479 using different units (fl. km⁻² yr⁻²) in the supplement supplementary information (Figs. S3 and S4 and S5). Figures S3 and S4
 480 and S5 show that the absolute lightning trends (fl. km⁻² yr⁻²) and the effects of global warming and increases in AeroPEs on
 481 the absolute lightning trends are slight in high-latitude regions- but prominent in tropical areas.



482



483

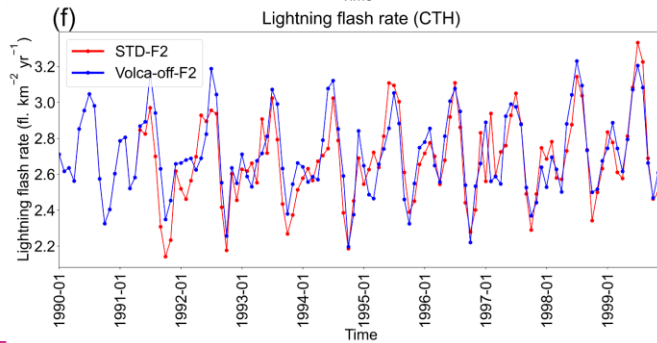
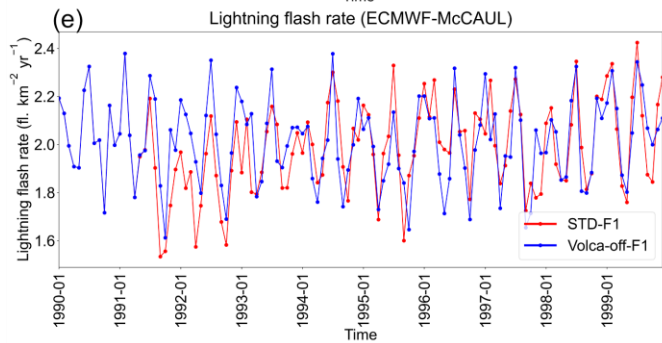
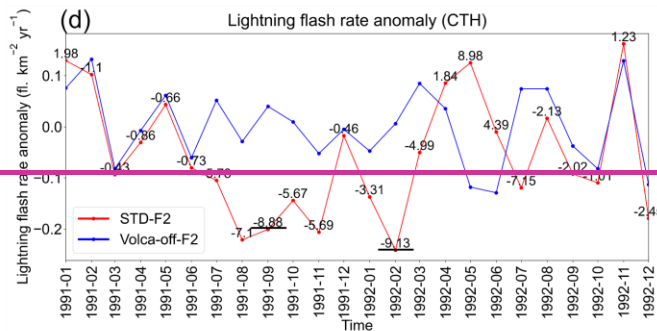
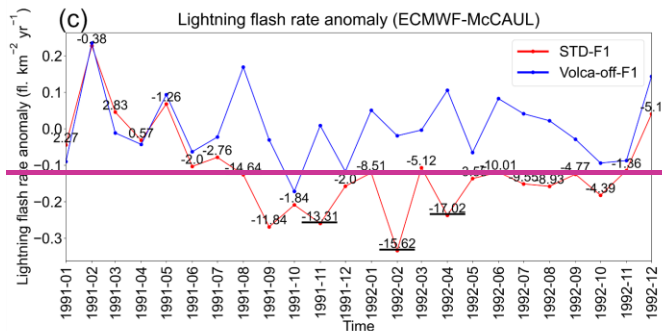
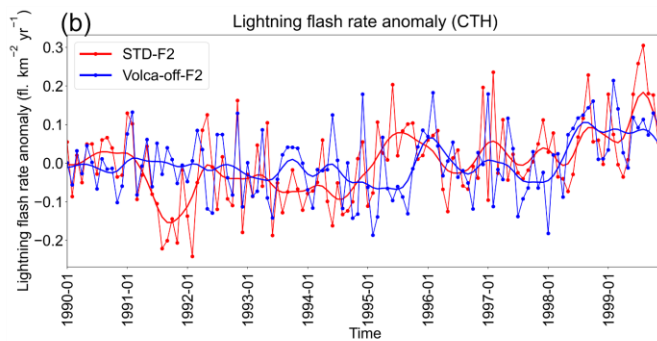
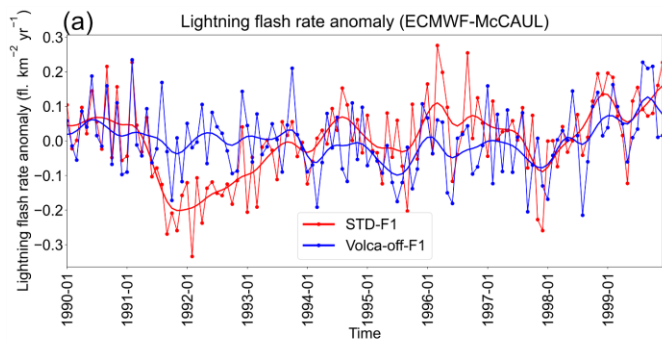
484 **Figure 89:** Time-series data of 1960–2014 annual global LNO_x production anomalies (TgN yr⁻¹) and their fitting curves simulated
 485 using the ECMWF-McCAUL scheme (a) and the CTH scheme (b). Trends of the fitting curves in percent per year are
 486 shown presented in the legends.

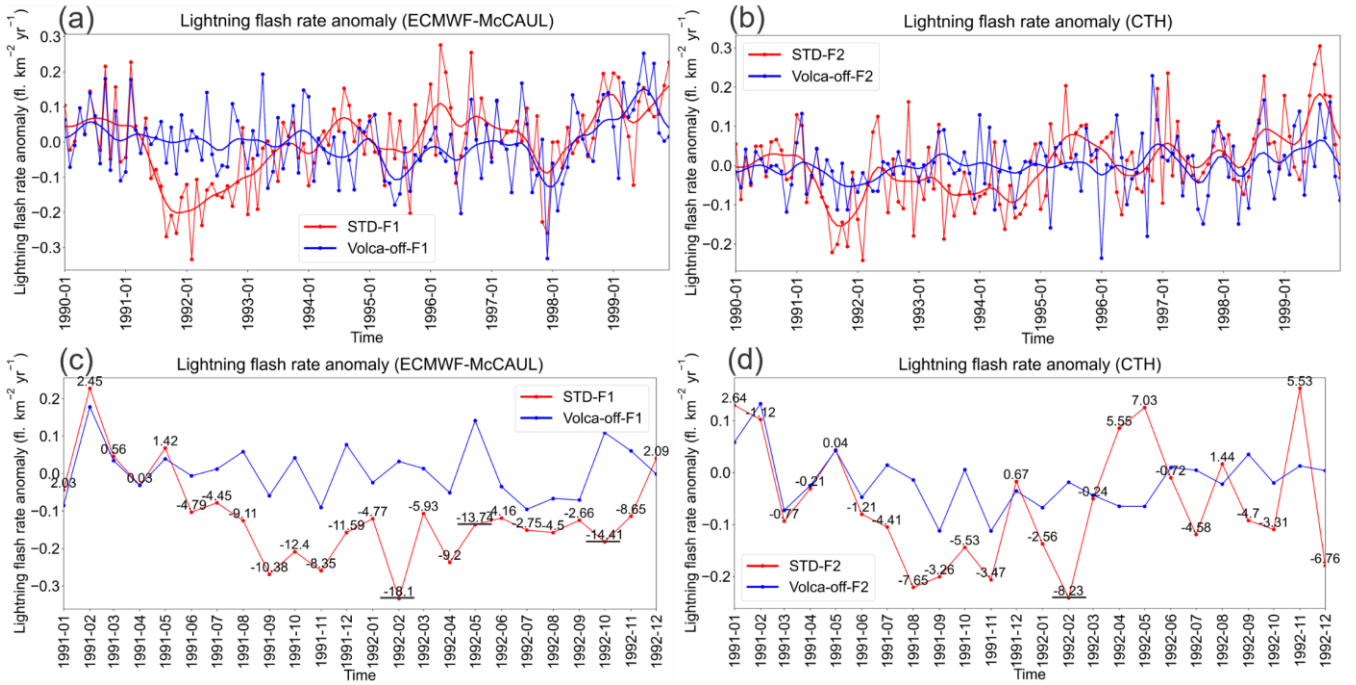
487

488 Trends in historical annual global LNO_x emissions for different scenarios are generally consistent with trends in historical
 489 global mean lightning flash rates LFRs, as shown in Figs. 4a–b, 5a–5b and Fig. 89. This finding is not surprising because, as the
 490 lightning NO_x emission parameterizations introduced in Sect. 2.2 show, the simulated lightning flash rates LFRs are linearly
 491 related to the simulated LNO_x emissions in our study. The results presented in Fig. 89 imply that historical global warming
 492 and increases in AeroPEs can affect atmospheric chemistry and can engender feedback by influencing LNO_x emissions.

493 3.3 Effects of Pinatubo volcanic eruption effects on historical lightning–LNO_x trends

494 We estimate the effects of the Pinatubo eruption effects on historical lightning–LNO_x trends and variation by comparing the
 495 simulation results of STD and Volca-off experiments. The simulated global mean lightning flash rates LFRs by STD and Volca-
 496 off experiments are the same until April 1991. They then begin to show differences from May 1991 (Figs. 9e–f). This The time
 497 series of global mean LFRs is not shown). This result is reasonable because the Pinatubo volcanic perturbations are removed
 498 from SAC during June 1991 through May 1994/1996 in the Volca-off experiments by equation (11), and because the SAC of
 499 May 1991 used in CHASER are is interpolated between the SAC of April 1991 and June 1991.





501

502 **Figure 910:** Time series of lightning flash rate or lightning flash rate LFR anomalies from during 1990 to 1999 or from during 1991
503 through 1992. Figures 9 Panels (a) and (b) show the time series of lightning flash rate LFR anomalies and their smoothed curves
504 by 1-D Gaussian (Denosing) filter from for 1990 through 1999. Figures 9 Panels (c) and (d) present the time series of lightning flash
505 rate LFR anomalies from during 1991 to 1992. The Values shown over the red lines in Figs. 9 panels (c) and (d) are Relative diff
506 calculated using equation 12.

507

508 Figures 9(e-f) show 10c-10d portray the time series of lightning flash rate during 1990-1999.

509

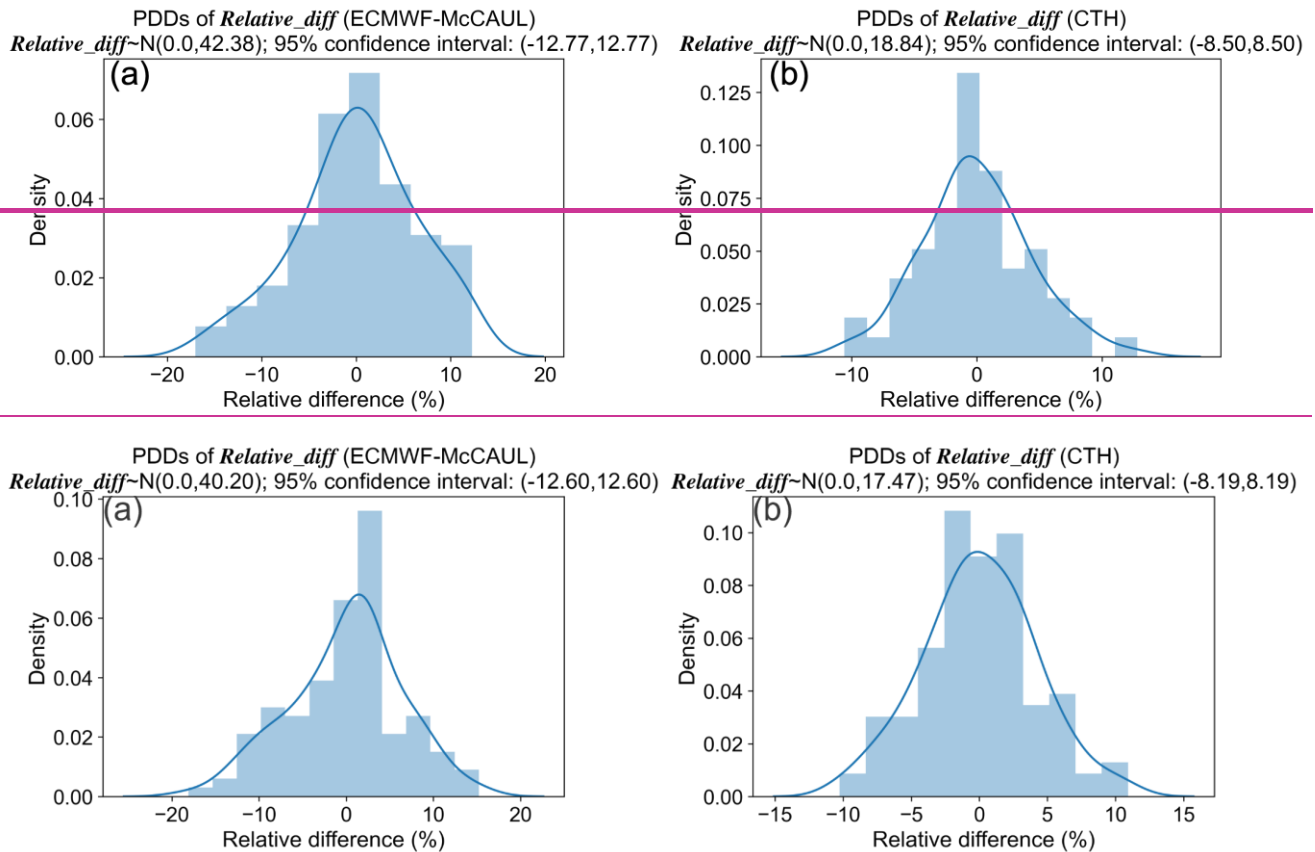
510 Figures 9c-d show the time series of lightning flash rate LFR anomalies and Relative diff (values over the red lines)
511 from during 1991 to 1992. Relative diff are relative differences of the global mean lightning flash rate LFR anomalies
512 between STD and Volca-off experiments calculated using the following equation.

513
$$\text{Relative_diff} = 100\% \times \frac{LFRA_{STD} - LFRA_{Volca-off}}{LFR_{Volca-off}} \quad (12)$$

514 In the equation, $LFRA_{STD}$ represents global mean lightning flash rate LFR anomalies simulated by STD-F1/F2 experiments.

515 $LFRA_{Volca-off}$ denotes global mean lightning flash rate LFR anomalies simulated by Volca-off-F1/F2 experiments.

516 $LFR_{Volca-off}$ symbolizes global mean lightning flash rates LFRs simulated by Volca-off-F1/F2 experiments.



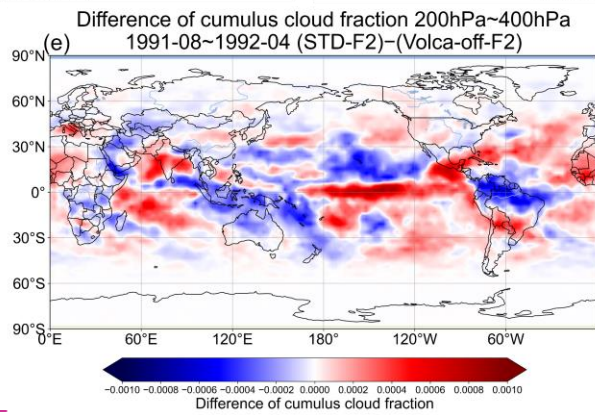
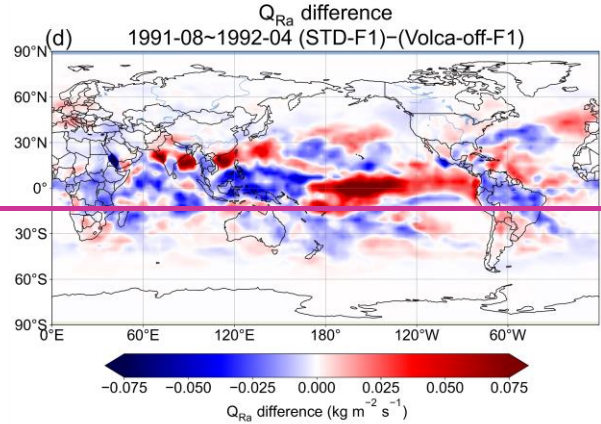
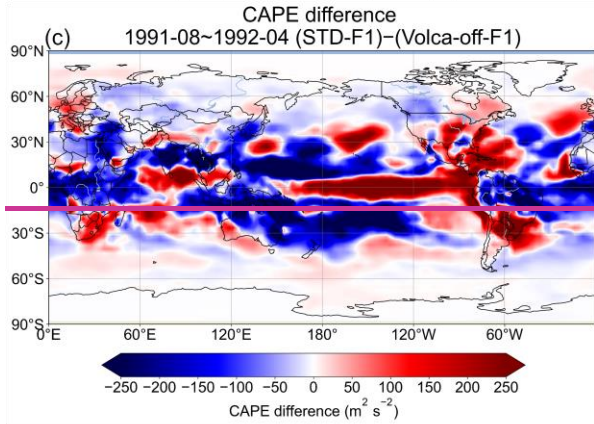
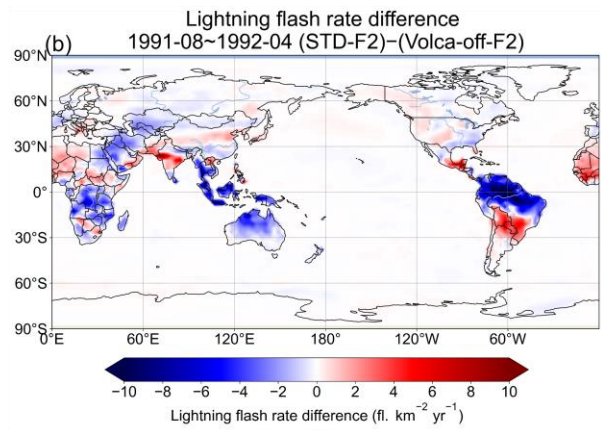
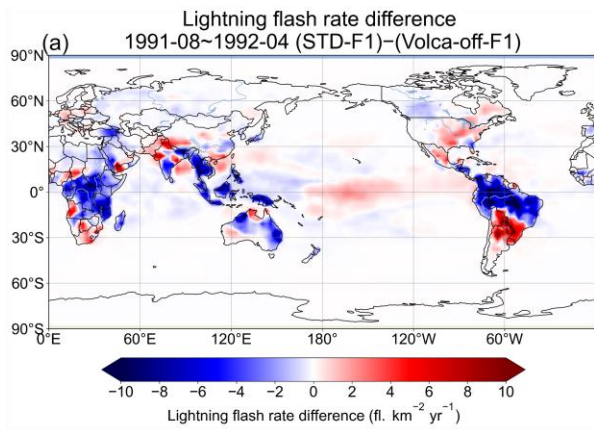
517

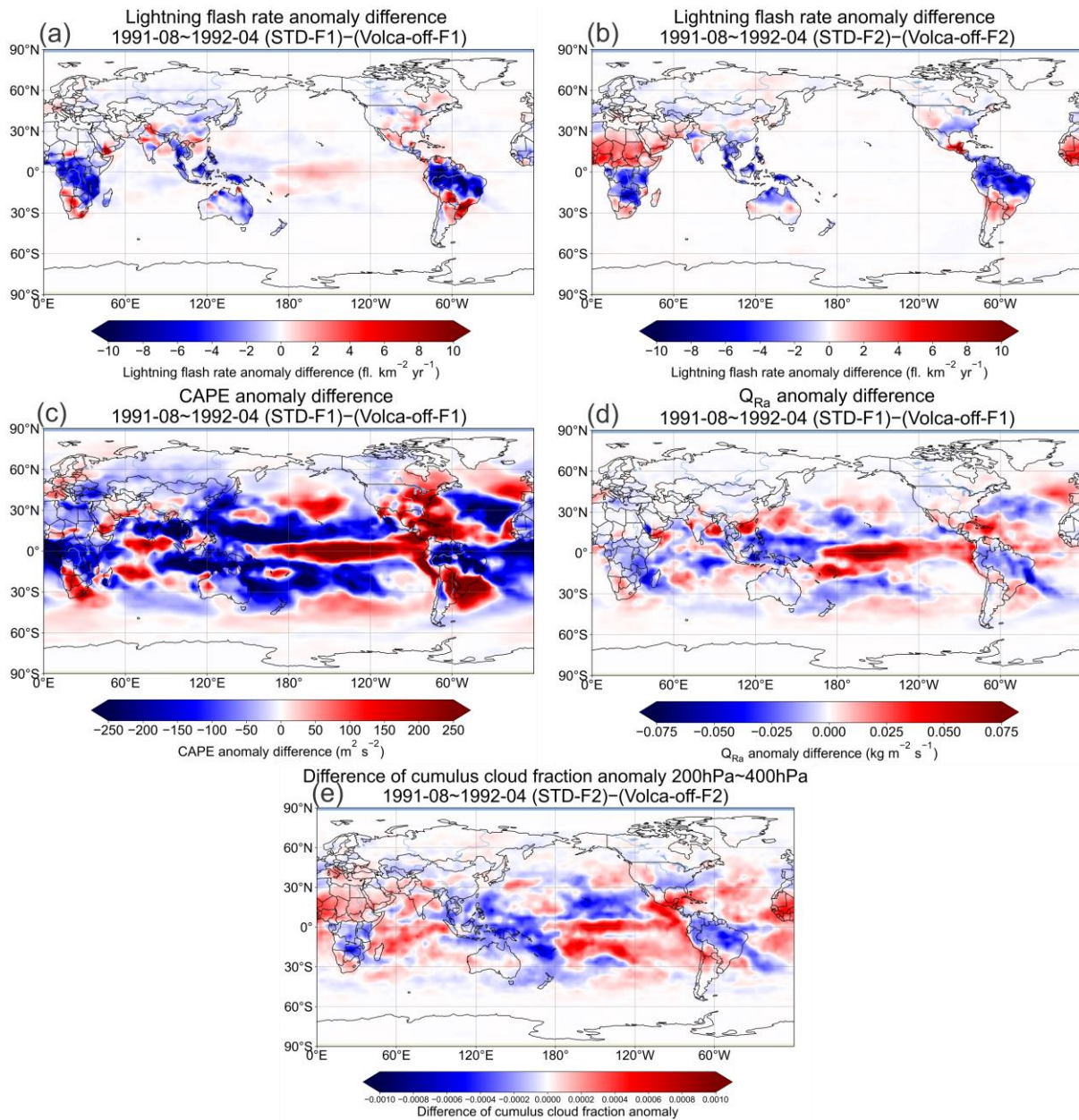
518

519 **Figure 4011:** Probability Density Distributions (PDDs) of *Relative_diff* obtained from monthly time-series data of *Relative_diff*
 520 during 1990–1999. The 95% confidence interval of *Relative_diff* is also shown in the titles of this figure.

521

522 The monthly time-series data of *Relative_diff* for 1990–1999 for both ~~of the~~ lightning schemes are calculated ~~and~~. The
 523 Probability Density Distributions (PDDs) of *Relative_diff* are displayed in Fig. 4011. The *Relative_diff* presented in
 524 Fig. 4011 are all normally distributed as determined by the Kolmogorov–Smirnov test. The 95% confidence interval of
 525 *Relative_diff* is calculated and shown in the titles of Fig. 4011. As displayed in Figs. ~~9e–d10c–10d~~, the underlined values
 526 (*Relative_diff*) ~~distributed within 1991–08–1992–04 outreached/exceeded~~ the 95% confidence interval, ~~which means there~~
 527 ~~are~~ indicating significant differences in the calculated global mean lightning flash rate LFR anomalies by STD and Volca-off
 528 experiments. In other words, global lightning activities were suppressed significantly by the Pinatubo eruption during the first
 529 year after the eruption.





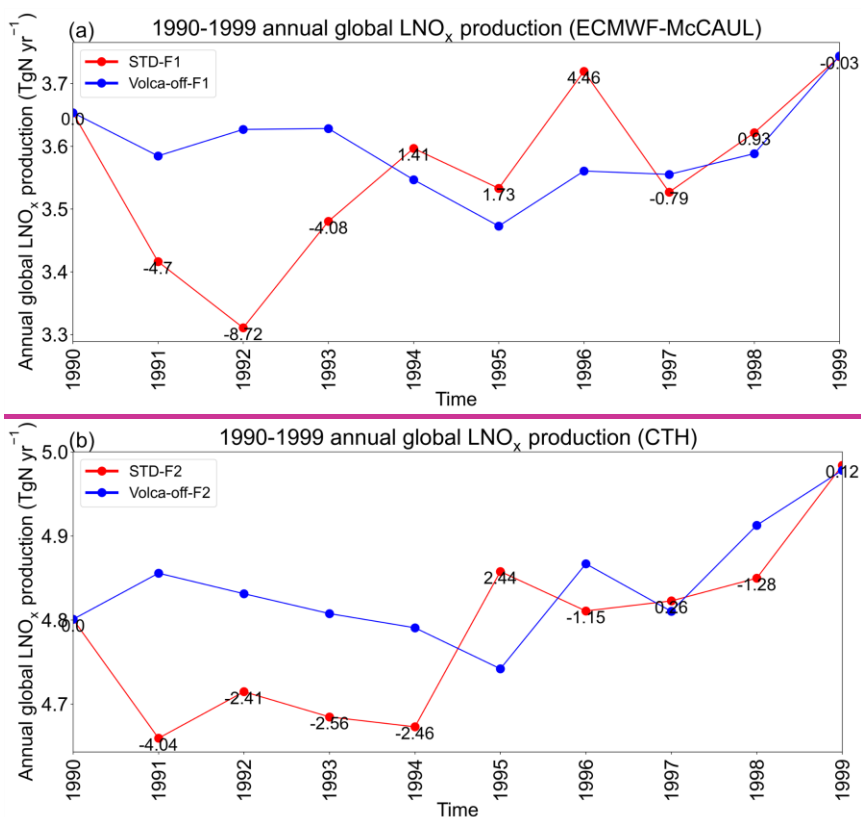
531

532 **Figure 11:** 1991-08 – 1992-04 averaged **lightning flash rate** **LFR anomaly** differences (a–b), CAPE **anomaly** differences (c), Q_{Ra}
 533 **anomaly** differences (d), and differences of 200 hPa – 400 hPa averaged cumulus cloud fraction **(e) anomaly** between STD-**F2** and
 534 **Volca-off-F2** experiments **(e)** on the global map.

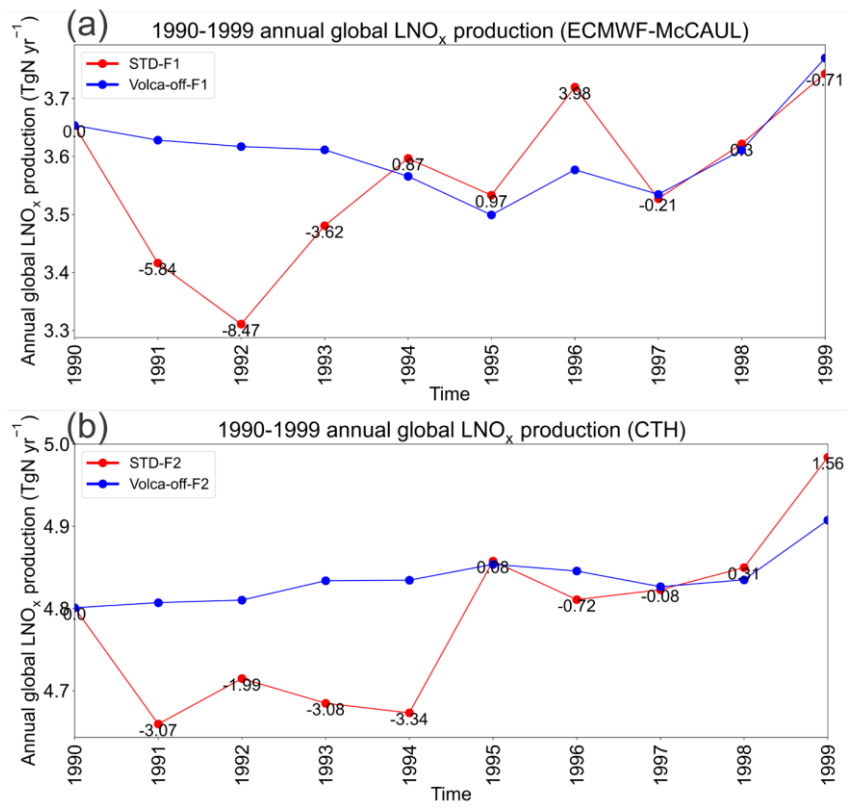
535

536 Figures 11a–11b show 1991-08 – 1992-04 averaged **lightning flash rate** **LFR anomaly** differences between STD and
 537 **Volca-off** experiments on the global map. We found from Figs. 11a–11b that lightning activities are suppressed

538 significantly within the three hotspots of lightning activities (Central Africa, Maritime Continent, and South America) during
 539 1991-08 – 1992-04, when the global mean lightning flash rates (LFRs) are found to be suppressed. To explore and elucidate the
 540 potential reasons for the suppressed global lightning activities during the first year after the Pinatubo eruption, we first
 541 investigated the 1991-08 – 1992-04 averaged differences in CAPE and Q_{Ra} differences (anomaly) between STD-F1 and Volca-
 542 off-F1 (Figs. 4e–4i, 12c–12d) because lightning densities are computed with CAPE and Q_{Ra} by the ECMWF-McCAUL scheme.
 543 Results showed that the Pinatubo eruption can lead to engender apparent reductions of CAPE and Q_{Ra} within tropical and
 544 subtropical terrestrial regions (typically three hotspots of lightning activities) where lightning occurrence is frequent. These
 545 reductions constitute the main reason for the suppressed global lightning activities during the first year after the Pinatubo
 546 eruption simulated by the ECMWF-McCAUL scheme. We also examined the 1991-08 – 1992-04 averaged differences of 200
 547 hPa – 400 hPa averaged cumulus cloud fraction anomaly between STD-F2 and Volca-off-F2 on the global map (Fig. 4e, 12e).
 548 The cumulus cloud fractions of each model layer are used to weight the calculated lightning densities from that layer by the
 549 CTH scheme, as explained in Sect. 2.2. As depicted in Fig. 4e, 12e and Fig. 5, 5, 6, the Pinatubo eruption led to marked
 550 reductions in the middle to upper tropospheric cumulus cloud fractions during 1991-08 – 1992-04 over three hotspots of
 551 lightning activities (Central Africa, Maritime Continent, and South America). As displayed in Fig. 5, 6, f, the cumulus that
 552 reached the middle to upper troposphere is highly related closely to lightning formation. Consequently, the simulated global
 553 lightning activities by the CTH scheme were also suppressed considerably during the first year after the Pinatubo eruption.



554



555

556 **Figure 4213:** 1990–1999 annual global LNO_x emissions calculated from the STD and Volca-off experiments' outputs simulated
 557 **by using** the ECMWF-McCAUL scheme (a) and the CTH scheme (b). Values over the red lines **are represent** the relative differences
 558 (%) between the red lines and blue lines, calculated with respect to the blue lines.

559

560 Aside from the **previously described** global lightning activity suppression **described earlier**, the production of LNO_x might also
 561 decrease after the Pinatubo eruption. To explore this conjecture, we compared the LNO_x emissions in STD and Volca-off
 562 experiments (Fig. 4213). In the case of the ECMWF-McCAUL scheme, the reduction of LNO_x emissions caused by the
 563 Pinatubo eruption started in 1991 (4.705.84%) and continued until 1993, with the highest percentage reduction occurring in
 564 1992 (8.7247%) (Fig. 42a13a). However, the CTH scheme showed a slightly different scenario of LNO_x emissions reduction
 565 after the Pinatubo eruption. The LNO_x emissions are almost evenly reduced during 1991–1994 in the case of the CTH scheme
 566 (Fig. 42b13b). In conclusion, our study indicates that the Pinatubo eruption can engender reductions in global LNO_x emissions,
 567 which last 2–3 years. However, there exists some uncertainty in evaluating the magnitude of the reductions (from 2.411.99%
 568 to 8.7247% for the annual percentage reduction found from our study).

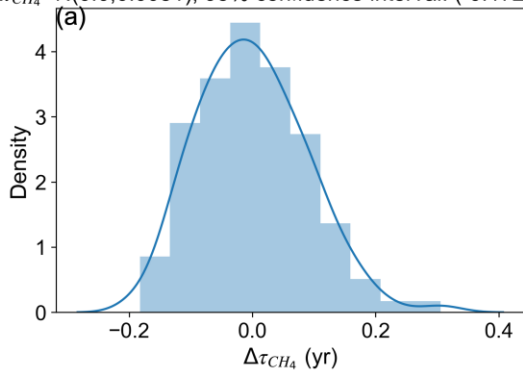
569

570 The simulated reduced global LNO_x emissions caused by the Pinatubo eruption might influence atmospheric chemistry
 571 significantly. Most importantly, the reduced global LNO_x emissions might reduce OH radical production and extend the global

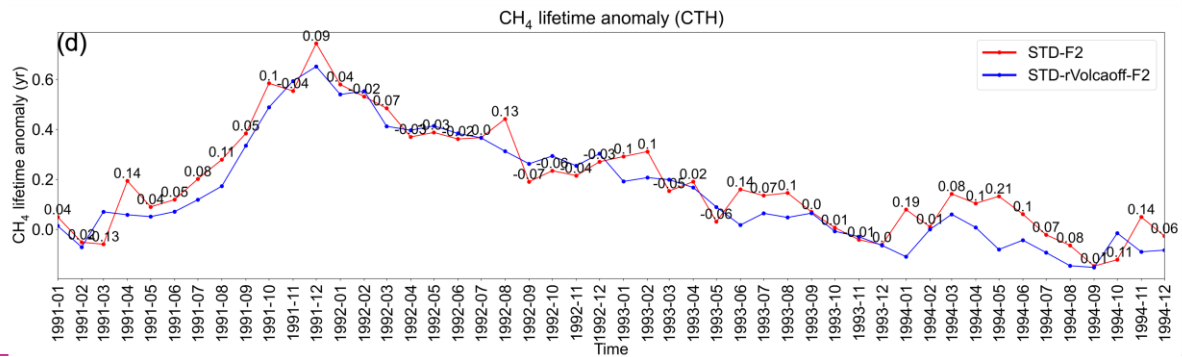
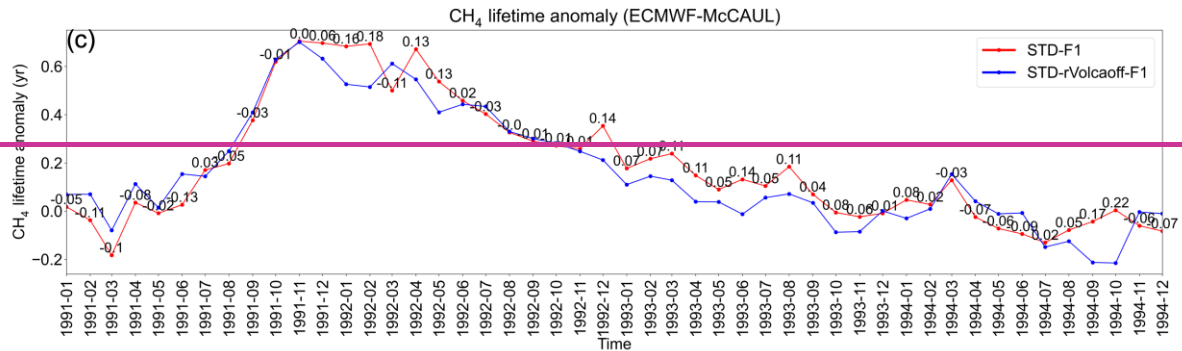
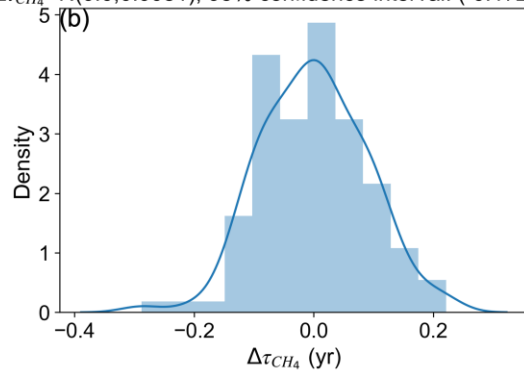
572 mean tropospheric lifetime of methane against tropospheric OH radical (~~-, abbreviated hereinafter abbreviated as the methane~~
573 ~~lifetime-).~~ We investigated this point further by comparing the methane lifetime anomaly simulated by STD and STD-rVolcaoff
574 experiments. As introduced in Sect. 2.5, the settings of STD-rVolcaoff experiments are the same as those use for STD
575 experiments, ~~for using that they use~~ the daily LNO_x emission rates calculated from the Volca-off experiments. We
576 calculated the monthly CH₄ lifetime anomalies during 1990–1999 and $\Delta\tau_{CH_4}$ (the difference of CH₄ lifetime anomaly between
577 STD and STD-rVolcaoff experiments), which are shown in Figs. ~~13e–d14c–14d~~. Figures ~~13a–b14a–14b~~ display the PDDs of
578 $\Delta\tau_{CH_4}$ monthly time series during 1990–1999. The $\Delta\tau_{CH_4}$ shown in Figs. ~~13a–b14a–14b~~ are all normally distributed, as
579 determined ~~by using~~ the Kolmogorov–Smirnov test. The 95% confidence interval of $\Delta\tau_{CH_4}$ is calculated and shown in the titles
580 of Figs. ~~13a–b14a–14b~~. The annual global LNO_x production averaged during 1990–1999 is 3.56 TgN yr⁻¹ for STD-F1 and 4.79
581 TgN yr⁻¹ for STD-F2. At this level of annual global LNO_x production, we found that within the first two years after the Pinatubo
582 eruption, the $\Delta\tau_{CH_4}$ ~~only slightly outreached exceeded~~ the 95% confidence interval ~~in 1992-02 (0.18 years)~~ simulated by ~~both~~
583 ~~lighting schemes (1992-02 and 1992-04 in the case of the ECMWF-McCAUL scheme-; 1991-12 in the case of the CTH~~
584 ~~scheme)~~. However, the widely cited range of annual global LNO_x production is 2–8 TgN yr⁻¹ (Schumann and Huntrieser, 2007).
585 Presuming that $\Delta\tau_{CH_4}$ ~~responds~~ linearly ~~responds~~ to the LNO_x emission level, and that the annual global LNO_x production is 8
586 TgN yr⁻¹, then the extension of ~~the~~ CH₄ lifetime because of the reduced LNO_x emissions can reach around 0.454 years for the
587 ECMWF-McCAUL scheme. As a comparison, ultraviolet shielding effects caused by stratospheric aerosols after the Pinatubo
588 eruption led to the maximum increase of the methane lifetime by about 0.6 years (Figs. ~~13e–d14c–14d~~).

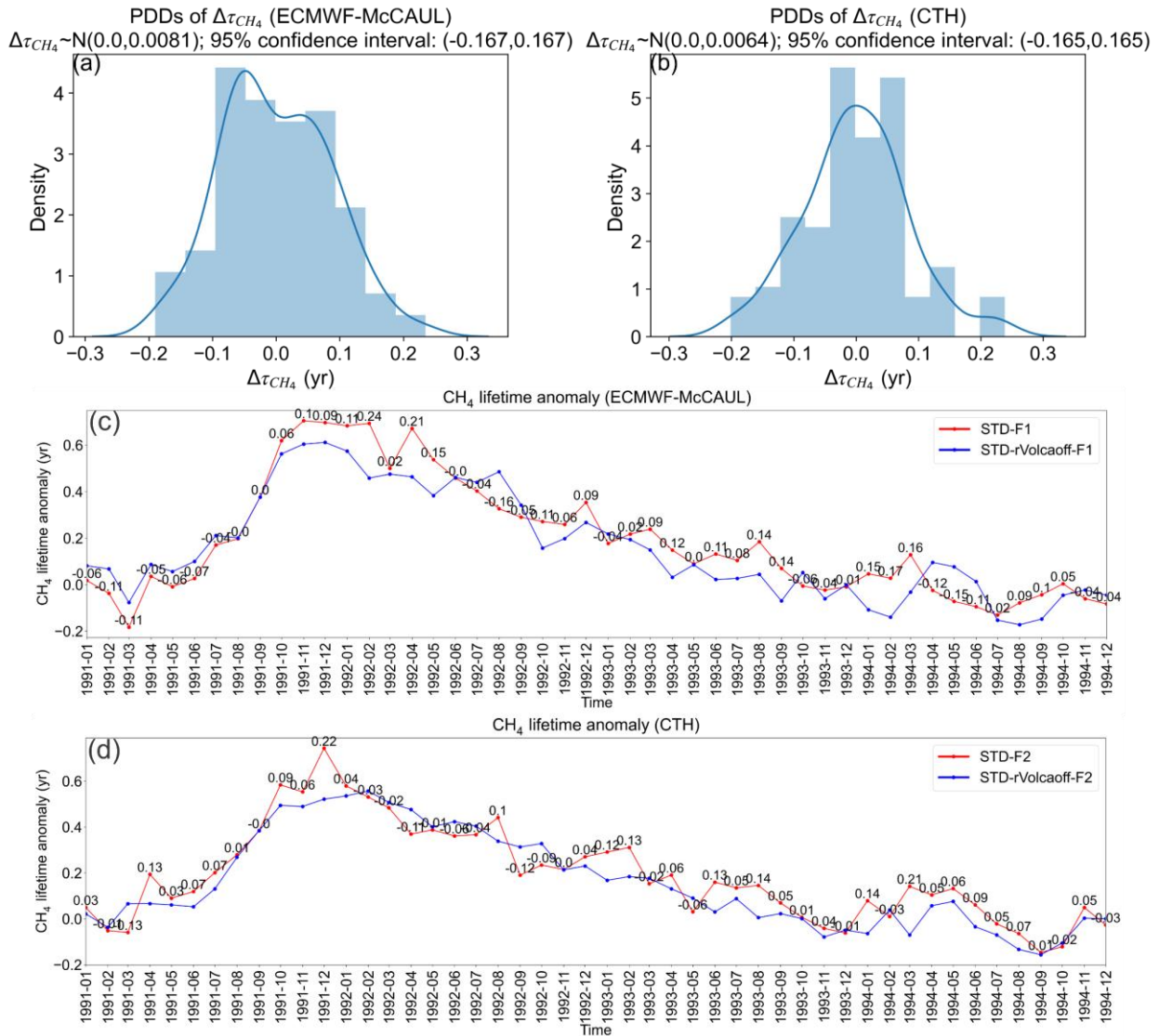
589

PDDs of $\Delta\tau_{CH_4}$ (ECMWF-McCAUL)
 $\Delta\tau_{CH_4} \sim N(0.0, 0.0081)$; 95% confidence interval: (-0.172, 0.172)



PDDs of $\Delta\tau_{CH_4}$ (CTH)
 $\Delta\tau_{CH_4} \sim N(0.0, 0.0081)$; 95% confidence interval: (-0.172, 0.172)





591

592 **Figure 13:14: Panels (a) and (b) show the Probability Density Distributions (PDDs) of $\Delta\tau_{CH_4}$ obtained from the monthly time series**
 593 **data of $\Delta\tau_{CH_4}$ during 1990–1999. $\Delta\tau_{CH_4}$ represents the difference in CH₄ lifetime anomaly between STD and STD-rVolcaoff**
 594 **experiments. The 95% confidence interval of $\Delta\tau_{CH_4}$ is also presented in the titles of Figs. 13a–panels (a)–(b). Panels (c) and (d)**
 595 **show monthly time series of CH₄ lifetime anomalies simulated by STD-F1/F2 and STD-rVolcaoff-F1/F2 experiments. Values over**
 596 **the red lines are the difference in CH₄ lifetime anomaly between STD and STD-rVolcaoff experiments ($\Delta\tau_{CH_4}$); represent $\Delta\tau_{CH_4}$.**

597 3.4 Model intercomparisons of lightning flash rate LFR trends with CMIP6 model outputs

598 The historical lightning trends demonstrated in our study are undoubtedly worth comparing with the results of other chemistry–
 599 climate models or Earth system models. As introduced in Sect. 2.4, for comparison of the simulated lightning flash rate LFR

600 trends and variations in our study with those of other CMIP6 models' outputs, we used all available ~~lightning flash rate~~LFR
601 data from the CMIP6 CMIP Historical experiments from CESM2-WACCM (3 ensembles) (Danabasoglu, 2019), GISS-E2-1-
602 G (9 ensembles) (Kelley et al., 2020), and UKESM1-0-LL (18 ensembles) (Tang et al., 2019). ~~Please refer to Table S1 for~~
603 ~~the presents a~~ complete list of the ensemble members ~~which were~~ used. It is noteworthy that the ~~lightning flash rate~~LFR data
604 obtained from the three ~~previously described~~ CMIP6 models ~~described earlier~~ are calculated using the CTH scheme. The
605 results of model intercomparisons of ~~lightning flash rate~~LFR trends and variations are displayed in Fig. ~~14~~15. As illustrated in
606 Figs. ~~14a–b~~15a–15b, both the ECMWF-McCAUL and the CTH schemes (STD-F1/F2) simulated almost flat statistically non-
607 significant global lightning trends, but the ensemble mean obtained from another three CMIP6 models exhibit significant
608 increasing global lightning trends (trends from 0.11% yr⁻¹ to 0.25% yr⁻¹). Many reasons ~~are responsible for~~underlie the
609 differences in global lightning trends simulated by CHASER in our study and by the three CMIP6 models, including the use
610 of different methods to determine SSTs/sea ice fields. Instead of using a coupled Atmosphere–Ocean general circulation model
611 to calculate SSTs/sea ice fields dynamically in the three CMIP6 models, CHASER uses the prescribed HadISST data (Rayner
612 et al., 2003), which are based on plenty of observational data. Changes in ~~the~~ global mean sea surface temperature ~~anomaly~~
613 during 1960–2014 (Δ SST) obtained from STD-F1/F2 and CMIP6 model outputs are ~~shown~~presented in Table 2. We also used
614 the observation-based Extended Reconstructed SST (ERSST) dataset (Huang et al., 2017) constructed by NOAA to evaluate
615 the Δ SST obtained from different models. The Δ SST calculated from ERSST during 1960–2014 is 0.543549°C, which ~~is~~ most
616 ~~close to~~close approximates the Δ SST obtained from STD-F1/F2. Considered from the perspective of SSTs/sea ice fields
617 alone, the results (global lightning trends) of our study are expected to be closer to the actual situation.

618
619 Actually, the three CMIP6 models simulated stronger global warming during 1960–2014 than CHASER in our study, as
620 displayed in Fig. ~~S6~~S7. The CTH scheme is reported to respond positively to simulated global warming (Price and Rind, 1994;
621 Zeng et al., 2008; Hui and Hong, 2013; Banerjee et al., 2014; Krause et al., 2014; Clark et al., 2017). The simulated stronger
622 global warming by the three CMIP6 models is regarded as responsible for differences in simulated global lightning trends
623 between our study and the three CMIP6 models (Figs. ~~14a–b~~15a–15b). We further investigated the sensitivities of the global
624 mean ~~lightning flash rate~~LFR anomaly change to the global mean surface temperature ~~anomaly~~ increase (% °C⁻¹) obtained
625 from CHASER and the three CMIP6 models. The sensitivities in percentage per degree Celsius are presented in Table 2.
626 Overall, even when using the same CTH scheme, the sensitivities (Δ LFR/ Δ TS) simulated by the three CMIP6 models are
627 higher than that simulated by CHASER in our study. This ~~different sensitivity~~ might be partially attributable to the nonlinear
628 relation between lightning response and climate change (Pinto, 2013; Krause et al., 2014). Compared to the CTH scheme, the
629 ECMWF-McCAUL scheme simulated a statistically non-significant negative sensitivity (Δ LFR/ Δ TS), which is attributable to
630 the stronger suppression of positive global lightning trends caused by increases in AeroPEs simulated ~~by using~~ the ECMWF-
631 McCAUL scheme.

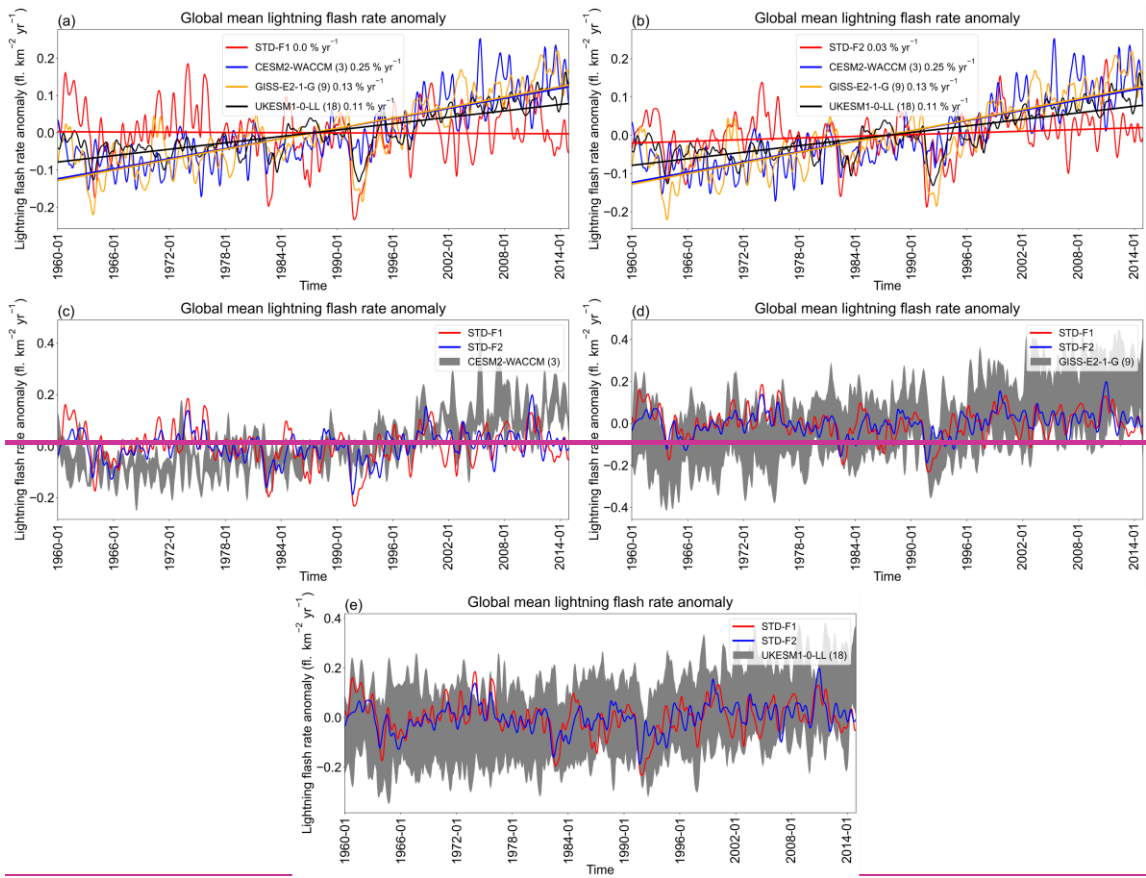
632

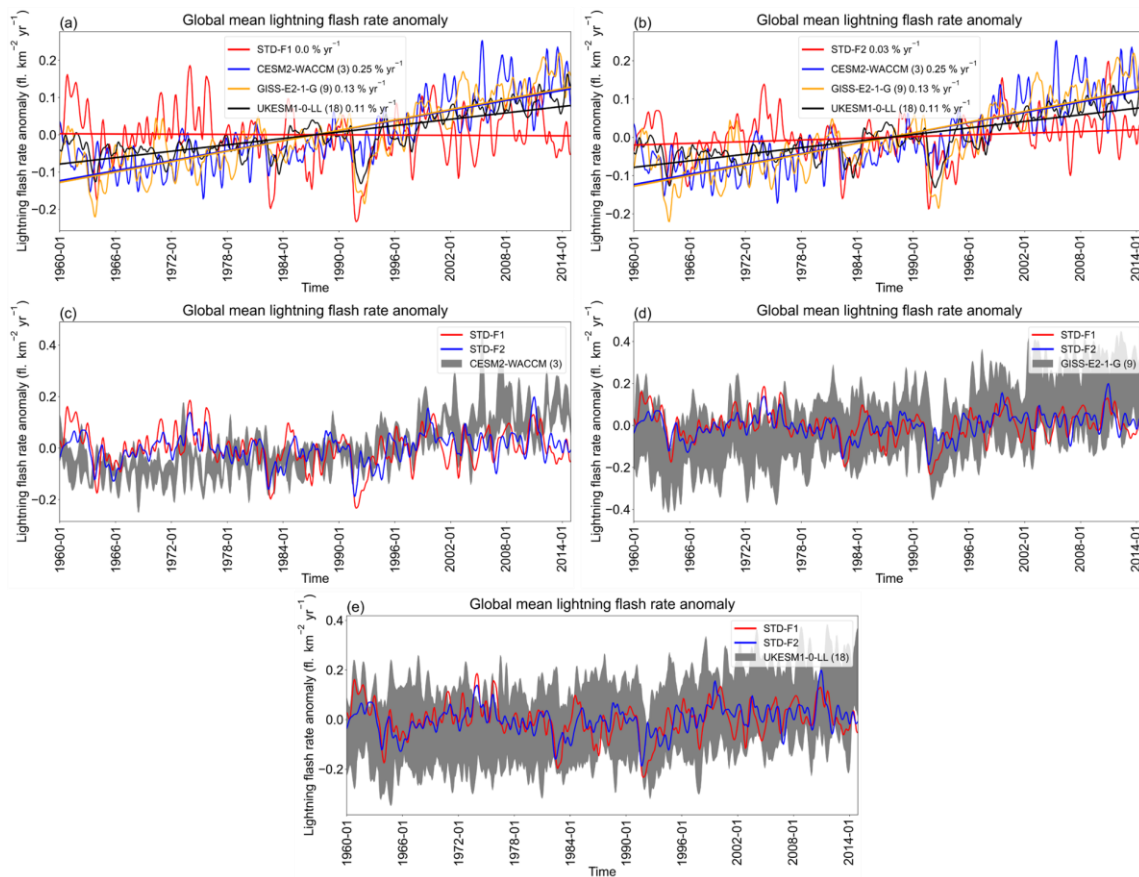
633 Table 2: Changes in global mean surface temperature anomaly (ΔTS), global mean sea surface temperature anomaly (ΔSST), global
634 mean lightning flash rate anomaly (ΔLFR), and the rate of change of ~~lightning flash rate~~LFR anomaly corresponding to each degree-
635 Celsius increase in global mean surface temperature anomaly ($\Delta LFR/\Delta TS$) obtained from STD-F1/F2 and CMIP6 model outputs.
636 The change of ΔSST obtained from the ERSST dataset is also shown in this Table. Changes were obtained by calculating the
637 difference between the rightmost and leftmost points of the approximating curve for the 1960–2014 time-series data.

Model/experiment/dataset	ΔTS ($^{\circ}C$)	ΔSST ($^{\circ}C$)	ΔLFR (%)	$\Delta LFR/\Delta TS$ ($\% \text{ } ^{\circ}C^{-1}$)
STD-F1	0.593	0.428	-0.272	-0.46
STD-F2	0.563	0.432	1.497	2.66
CESM2-WACCM	1.245	1.077	13.758	11.05
GISS-E2-1-G	0.810	0.677	7.248	8.95
UKESM1-0-LL	1.141	0.999	5.942	5.21
ERSST	—	0.549	—	—

638

639 Figures ~~14d–e~~15d–15e affirm that the global lightning variation simulated by our study is basically within the full ensemble
640 range of GISS-E2-1-G and UKESM1-0-LL. After the Pinatubo eruption, as described in Sect. 3.3 of this report, the GISS-E2-
641 1-G and UKESM1-0-LL models also manifest significant suppression of global lightning activities, but the CESM2-WACCM
642 model ~~does not show this~~shows no such phenomenon. The commonalities as well asand differences in global lightning trends
643 and variations found in the model intercomparisons imply that great uncertainties existed in past (1960–2014) global lightning
644 trend simulations. Such uncertainties deserve to be investigated further.





646

647 **Figure 1415:** Comparisons of simulated global mean lightning flash rate LFR anomalies found in our study (CHASER) and found
 648 using other CMIP6 models. All the figures are created based on the monthly time-series data of global mean lightning flash rate LFR
 649 anomalies with a 1-D Gaussian (Denoising) filter applied. For CMIP6 models, the ensemble mean is shown as the solid line, and the
 650 full ensemble range is shown as grey shading (c–e). Fitting curves and the trends of fitting curves ($\% \text{ yr}^{-1}$) are also given in (a–b).

651 **4 Discussions**Discussion and Conclusions

652 We used two lightning schemes (the CTH and ECMWF-McCAUL schemes) to study historical (1960–2014) lightning–LNO_x
 653 trends and variations and their controlling/influencing factors (global warming, increases in AeroPEs, and Pinatubo eruption)
 654 within the CHASER (MIROC) chemistry–climate model. The CTH scheme, which is the most widely used lightning scheme,
 655 but it nevertheless lacks a direct physical link with the charging mechanism. The ECMWF-McCAUL scheme is a newly
 656 developed process-based/ice-based lightning scheme with a direct physical link to the charging mechanism.

657

658 With only the aerosol radiative effects considered in the lightning–aerosols interaction, both lightning schemes simulated
 659 almost flat trends of global mean lightning flash rate LFR during 1960–2014. Reportedly, because the aerosol microphysical

660 effects can enhance lightning activities (Yuan et al., 2011; Wang et al., 2018; Liu et al., 2020), our study might underestimate
661 the increasing trend of global mean ~~lightning flash rate~~ LFR (our study only considered the aerosol radiative effects in aerosol–
662 lightning interactions). Further research is ~~expected~~~~considering~~~~anticipated~~, with consideration of the effects of aerosol
663 microphysical effects on long-term lightning trends. Moreover, both lightning schemes manifest that past global warming
664 enhances the historical trend of global mean lightning density toward the positive direction (around $0.03\% \text{ yr}^{-1}$ or $3\% \text{ K}^{-1}$).
665 However, past increases in AeroPEs exert the opposite effect to the lightning trend ($-0.07\% \text{ yr}^{-1} - -0.04\% \text{ yr}^{-1}$). The effects of
666 the ~~increases in~~increased AeroPEs on the lightning trend only over land regions expand to $-0.10\% \text{ yr}^{-1} - -0.05\% \text{ yr}^{-1}$, which
667 implies that the effects are more significant over land regions. We obtained similar results for the historical global LNO_x
668 emissions trend, which indicates that historical global warming and increases in AeroPEs can affect atmospheric chemistry
669 and engender feedback by influencing LNO_x emissions. Although the CTH and ECMWF-McCAUL schemes use different
670 parameters to simulate lightning, both lightning schemes indicate that the enhanced global convective activity under global
671 warming is the main reason for the increase in lightning– LNO_x emissions. In contrast, the increases in AeroPEs have decreased
672 lightning– LNO_x emissions by weakening the convective activity in the ~~hotspots of~~ lightning hotspots. By analyzing the
673 simulation results on the global map, we also found that the effects of historical global warming and increases in AeroPEs on
674 lightning trends are heterogeneous across different regions. Our results indicate that historical global warming enhances
675 lightning activities within the Arctic region and Japan but suppresses lightning activities around New Zealand and some parts
676 of the Southern Ocean. Both lightning schemes demonstrated that the historical increases in AeroPEs suppress lightning
677 activities in some parts of the Southern Ocean and South America. The ECMWF-McCAUL scheme also suggests that historical
678 increases in AeroPEs suppress lightning activities in some parts of India and China: when only the aerosol radiative effects are
679 considered. This finding is plausible because both countries experienced dramatic increases in AeroPEs during 1960–2014
680 because of rapid economic growth.

681

682 Furthermore, this report is the first describing ~~that~~significant suppression of global lightning activity ~~was suppressed~~
683 significantly during the first year after the Pinatubo eruption, which is indicated in both lightning schemes (global lightning
684 activities decreased by up to ~~17.02~~18.10% simulated by the ECMWF-McCAUL scheme). This finding is mainly attributable
685 to the Pinatubo eruption weakening of the convective activities within the hotspots of lightning, which in turn decreased ~~the~~
686 ~~amount of column precipitating ice~~ (Q_{Ra}) Q_{Ra} and middle-level to high-level cumulus cloud fractions in these regions. The
687 simulation results also indicate that the Pinatubo eruption can engender reductions in global LNO_x emissions, which last 2–3
688 years. However, some uncertainty exists in evaluating magnitude of these reductions (from ~~2.41~~1.99% to ~~8.72~~4.7% for the
689 annual percentage reduction in our study). The case study of the Pinatubo eruption in our research indicates that other large-
690 scale volcanic eruptions can also engender significant reduction of global lightning activities and global-scale LNO_x emissions.

691

692 Lastly, we compared the global lightning trends demonstrated in our study with the outputs of three CMIP6 models: CESM2-
693 WACCM, GISS-E2-1-G, and UKESM1-0-LL. We used all available ~~lightning flash rate~~ LFR data from the CMIP6 CMIP

694 historical experiments from the three models described above. The three CMIP6 models ~~suggested~~suggest significant
695 increasing trends in historical global lightning activities, which differs from the findings of our study. Unlike the three CMIP6
696 models ~~that~~which use a coupled Atmosphere–Ocean general circulation model to calculate SSTs/sea ice fields dynamically,
697 our study (CHASER) uses the prescribed HadISST SSTs/sea ice data, which ~~are closer to~~more closely reflect the actual
698 situation. Therefore, we believe that the results (the historical global lightning trends) obtained from our study (CHASER) ~~are~~
699 ~~closer to~~more closely approximate the actual situation. However, model intercomparisons of global lightning trends still
700 indicate that ~~significant~~considerable uncertainties exist in ~~the~~ historical (1960–2014) global lightning trend simulations, and
701 that such uncertainties deserve further investigation.

702 **Code availability**

703 The source code for CHASER to reproduce results obtained from this work is obtainable from the repository at
704 <https://doi.org/10.5281/zenodo.5835796> (He et al., 2022a).

705 **Data availability**

706 The LIS/OTD data used for this study are available from <https://ghrc.nsstc.nasa.gov/hydro/?q=LRTS> (last access: 11 January
707 2022). The CMIP6 model outputs (~~lightning flash rate~~LFR and surface temperature) used for this study are available from
708 <https://aims2.llnl.gov/search> (last access: 1 February 2023). The Extended Reconstructed SST data used for this study are
709 available from <https://www.ncei.noaa.gov/products/extended-reconstructed-sst> (last access: 27 March 2023).

710 **Author ~~contribution~~contributions**

711 YFH conducted all simulations, interpreted the results, and wrote the manuscript. KS developed the CHASER (MIROC) model
712 code, conceived the presented idea, and supervised the findings of this work and the manuscript preparation.

713 **Competing interests**

714 The authors declare that they have no conflict of interest.

715 **Acknowledgments**

716 This research was supported by the Global Environment Research Fund (S–12 and S–20) of the Ministry of the Environment
717 (MOE), Japan, and JSPS KAKENHI Grant Numbers: JP20H04320, JP19H05669, and JP19H04235. This work was supported
718 by the Japan Science and Technology Agency (JST) Support for Pioneering Research Initiated by the Next Generation

719 (SPRAINING), Grant Number JPMJSP2125. The author would like to take this opportunity to thank the “Interdisciplinary
720 Frontier Next-Generation Researcher Program of the Tokai Higher Education and Research System.” The simulations were
721 completed **withusing** the supercomputer (NEC SX-Aurora TSUBASA) at NIES (Japan). We thank NASA scientists and staff
722 for providing LIS/OTD lightning observation data. We acknowledge the World Climate Research Programme, which
723 coordinated and promoted CMIP6 through its Working Group on Coupled Modelling. We extend our sincere gratitude to the
724 climate modelling groups for producing and providing their model outputs, to the Earth System Grid Federation (ESGF) for
725 archiving the data and providing free downloads, and to the multiple funding agencies that have supported the CMIP6 as well
726 as the Earth System Grid Federation. We also thank Ms. Do Thi Nhu Ngoc for her assistance in downloading the CMIP6
727 model outputs.

728 **References**

- 729 Allen, D. J., Pickering, K. E., Bucsela, E., Krotkov, N., and Holzworth, R.: Lightning NO_x Production in the Tropics as
730 Determined Using OMI NO₂ Retrievals and WWLLN Stroke Data, *Journal of Geophysical Research: Atmospheres*,
731 124, 13498–13518, <https://doi.org/10.1029/2018JD029824>, 2019.
- 732 Altaratz, O., Kucienska, B., Kostinski, A., Raga, G. B., and Koren, I.: Global association of aerosol with flash density of
733 intense lightning, *Environ. Res. Lett.*, 12, 114037, <https://doi.org/10.1088/1748-9326/aa922b>, 2017.
- 734 Arfeuille, F., Luo, B. P., Heckendorn, P., Weisenstein, D., Sheng, J. X., Rozanov, E., Schraner, M., Brönnimann, S., Thomason,
735 L. W., and Peter, T.: Modeling the stratospheric warming following the Mt. Pinatubo eruption: uncertainties in aerosol
736 extinctions, *Atmospheric Chemistry and Physics*, 13, 11221–11234, <https://doi.org/10.5194/acp-13-11221-2013>, 2013.
- 737 Banerjee, A., Archibald, A. T., Maycock, A. C., Telford, P., Abraham, N. L., Yang, X., Braesicke, P., and Pyle, J. A.: Lightning
738 NO_x, a key chemistry–climate interaction: Impacts of future climate change and consequences for tropospheric oxidising
739 capacity, *Atmospheric Chemistry and Physics*, 14, 9871–9881, <https://doi.org/10.5194/acp-14-9871-2014>, 2014.
- 740 Boccippio, D. J., Koshak, W. J., and Blakeslee, R. J.: Performance Assessment of the Optical Transient Detector and Lightning
741 Imaging Sensor. Part I: Predicted Diurnal Variability, *Journal of Atmospheric and Oceanic Technology*, 19, 1318–1332,
742 [https://doi.org/10.1175/1520-0426\(2002\)019<1318:PAOTOT>2.0.CO;2](https://doi.org/10.1175/1520-0426(2002)019<1318:PAOTOT>2.0.CO;2), 2002.
- 743 Boucher, O.: *Atmospheric Aerosols*, Springer Netherlands, Dordrecht, <https://doi.org/10.1007/978-94-017-9649-1>, 2015.
- 744 Bucsela, E. J., Pickering, K. E., Allen, D. J., Holzworth, R. H., and Krotkov, N. A.: Midlatitude Lightning NO_x Production
745 Efficiency Inferred From OMI and WWLLN Data, *Journal of Geophysical Research: Atmospheres*, 124, 13475–13497,
746 <https://doi.org/10.1029/2019JD030561>, 2019.
- 747 Cecil, D. J., Buechler, D. E., and Blakeslee, R. J.: Gridded lightning climatology from TRMM-LIS and OTD: Dataset
748 description, *Atmospheric Research*, 135–136, 404–414, <https://doi.org/10.1016/j.atmosres.2012.06.028>, 2014.
- 749 Cerveny, R. S., Bessemoulin, P., Burt, C. C., Cooper, M. A., Cunjie, Z., Dewan, A., Finch, J., Holle, R. L., Kalkstein, L.,
750 Kruger, A., Lee, T., Martínez, R., Mohapatra, M., Pattanaik, D. R., Peterson, T. C., Sheridan, S., Trewin, B., Tait, A.,

751 and Wahab, M. M. A.: WMO Assessment of Weather and Climate Mortality Extremes: Lightning, Tropical Cyclones,
752 Tornadoes, and Hail, *Weather, Climate, and Society*, 9, 487–497, <https://doi.org/10.1175/WCAS-D-16-0120.1>, 2017.

753 Clark, S. K., Ward, D. S., and Mahowald, N. M.: Parameterization-based uncertainty in future lightning flash density,
754 *Geophysical Research Letters*, 44, 2893–2901, <https://doi.org/10.1002/2017GL073017>, 2017.

755 NOAA National Centers for Environmental Information (NCEI), *Climate at a Glance: Global Time Series*, published June
756 2023, retrieved on January 10, 2023 from [https://www.ncei.noaa.gov/access/monitoring/climate-at-a-](https://www.ncei.noaa.gov/access/monitoring/climate-at-a-glance/global/time-series/globe/land_ocean/3/8/1880-2020)
757 [glance/global/time-series/globe/land_ocean/3/8/1880-2020](https://www.ncei.noaa.gov/access/monitoring/climate-at-a-glance/global/time-series/globe/land_ocean/3/8/1880-2020).

758 Cooper, M. A. and Holle, R. L.: Current Global Estimates of Lightning Fatalities and Injuries, in: *Reducing Lightning Injuries*
759 *Worldwide*, edited by Cooper, M. A. and Holle, R. L., Springer International Publishing, Cham, 65–73,
760 https://doi.org/10.1007/978-3-319-77563-0_6, 2019.

761 Cooray, V., Rahman, M., and Rakov, V.: On the NO_x production by laboratory electrical discharges and lightning, *Journal of*
762 *Atmospheric and Solar–Terrestrial Physics*, 71, 1877–1889, <https://doi.org/10.1016/j.jastp.2009.07.009>, 2009.

763 Danabasoglu, G.: NCAR CESM2-WACCM model output prepared for CMIP6 CMIP historical,
764 <https://doi.org/10.22033/ESGF/CMIP6.10071>, 2019.

765 Danabasoglu, G., Lamarque, J.-F., Bacmeister, J., Bailey, D. A., DuVivier, A. K., Edwards, J., Emmons, L. K., Fasullo, J.,
766 Garcia, R., Gettelman, A., Hannay, C., Holland, M. M., Large, W. G., Lauritzen, P. H., Lawrence, D. M., Lenaerts, J.
767 T. M., Lindsay, K., Lipscomb, W. H., Mills, M. J., Neale, R., Oleson, K. W., Otto-Bliesner, B., Phillips, A. S., Sacks,
768 W., Tilmes, S., van Kampenhout, L., Vertenstein, M., Bertini, A., Dennis, J., Deser, C., Fischer, C., Fox-Kemper, B.,
769 Kay, J. E., Kinnison, D., Kushner, P. J., Larson, V. E., Long, M. C., Mickelson, S., Moore, J. K., Nienhouse, E., Polvani,
770 L., Rasch, P. J., and Strand, W. G.: The Community Earth System Model Version 2 (CESM2), *Journal of Advances in*
771 *Modeling Earth Systems*, 12, e2019ms001916, <https://doi.org/10.1029/2019ms001916>, 2020.

772 Del Genio, A. D., Yao, M.-S., and Jonas, J.: Will moist convection be stronger in a warmer climate?, *Geophysical Research*
773 *Letters*, 34, <https://doi.org/10.1029/2007GL030525>, 2007.

774 Finney, D. L., Doherty, R. M., Wild, O., and Abraham, N. L.: The impact of lightning on tropospheric ozone chemistry using
775 a new global lightning parametrisation, *Atmospheric Chemistry and Physics*, 16, 7507–7522,
776 <https://doi.org/10.5194/acp-16-7507-2016>, 2016b.

777 Finney, D. L., Doherty, R. M., Wild, O., Huntrieser, H., Pumphrey, H. C., and Blyth, A. M.: Using cloud ice flux to parametrise
778 large-scale lightning, *Atmospheric Chemistry and Physics*, 14, 12665–12682, [https://doi.org/10.5194/acp-14-12665-](https://doi.org/10.5194/acp-14-12665-2014)
779 [2014](https://doi.org/10.5194/acp-14-12665-2014), 2014.

780 Finney, D. L., Doherty, R. M., Wild, O., Stevenson, D. S., MacKenzie, I. A., and Blyth, A. M.: A projected decrease in
781 lightning under climate change, *Nature Climate Change*, 8, 210–213, <https://doi.org/10.1038/s41558-018-0072-6>, 2018.

782 Finney, D. L., Doherty, R. M., Wild, O., Young, P. J., and Butler, A.: Response of lightning NO_x emissions and ozone
783 production to climate change: Insights from the Atmospheric Chemistry and Climate Model Intercomparison Project,
784 *Geophysical Research Letters*, 43, 5492–5500, <https://doi.org/10.1002/2016GL068825>, 2016a.

785 Fujibe, F.: Long-term Change in Lightning Mortality and Its Relation to Annual Thunder Days in Japan, *Journal of Natural*
786 *Disaster Science*, 38, 17–29, <https://doi.org/10.2328/jnds.38.17>, 2017.

787 Goodman, S. J., Buechler, D. E., and Wright, P. D.: Lightning/rainfall relationships during COHMEX, NTRS Author
788 Affiliations: NASA Marshall Space Flight Center, Universities Space Research Association NTRS Document ID:
789 19900057799 NTRS Research Center: Legacy CDMS (CDMS), 1990.

790 Goto, D., Nakajima, T., Dai, T., Takemura, T., Kajino, M., Matsui, H., Takami, A., Hatakeyama, S., Sugimoto, N., Shimizu,
791 A., and Ohara, T.: An evaluation of simulated particulate sulfate over East Asia through global model intercomparison,
792 *Journal of Geophysical Research: Atmospheres*, 120, 6247–6270, <https://doi.org/10.1002/2014JD021693>, 2015.

793 Guenther, A. B., Jiang, X., Heald, C. L., Sakulyanontvittaya, T., Duhl, T., Emmons, L. K., and Wang, X.: The Model of
794 Emissions of Gases and Aerosols from Nature ver. 2.1 (MEGAN2.1): an extended and updated framework for modeling
795 biogenic emissions, *Geosci. Model Dev.*, 5, 1471–1492, <https://doi.org/10.5194/gmd-5-1471-2012>, 2012.

796 Ha, P. T. M., Matsuda, R., Kanaya, Y., Taketani, F., and Sudo, K.: Effects of heterogeneous reactions on tropospheric
797 chemistry: A global simulation with the chemistry–climate model CHASER V4.0, *Geoscientific Model Development*,
798 14, 3813–3841, <https://doi.org/10.5194/gmd-14-3813-2021>, 2021.

799 He, Y., Hoque, M. S. H., and Sudo, K.: Introducing new lightning schemes into the CHASER (MIROC) chemistry climate
800 model, [Code], Zenodo, <https://doi.org/10.5281/zenodo.5835796>, 2022a.

801 He, Y., Hoque, H. M. S., and Sudo, K.: Introducing new lightning schemes into the CHASER (MIROC) chemistry–climate
802 model, *Geoscientific Model Development*, 15, 5627–5650, <https://doi.org/10.5194/GMD-15-5627-2022>, 2022b.

803 Hoesly, R. M., Smith, S. J., Feng, L., Klimont, Z., Janssens-Maenhout, G., Pitkanen, T., Seibert, J. J., Vu, L., Andres, R. J.,
804 Bolt, R. M., Bond, T. C., Dawidowski, L., Kholod, N., Kurokawa, J., Li, M., Liu, L., Lu, Z., Moura, M. C. P., O’Rourke,
805 P. R., and Zhang, Q.: Historical (1750–2014) anthropogenic emissions of reactive gases and aerosols from the
806 Community Emissions Data System (CEDS), *Geosci. Model Dev.*, 11, 369–408, [https://doi.org/10.5194/gmd-11-369-](https://doi.org/10.5194/gmd-11-369-2018)
807 2018, 2018.

808 Huang, B., Thorne, P. W., Banzon, V. F., Boyer, T., Chepurin, G., Lawrimore, J. H., Menne, M. J., Smith, T. M., Vose, R. S.,
809 and Zhang, H.-M.: Extended Reconstructed Sea Surface Temperature, Version 5 (ERSSTv5): Upgrades, Validations,
810 and Intercomparisons, *Journal of Climate*, 30, 8179–8205, <https://doi.org/10.1175/JCLI-D-16-0836.1>, 2017.

811 Hui, J. and Hong, L.: Projected Changes in NO_x Emissions from Lightning as a Result of 2000–2050 Climate Change,
812 *Atmospheric and Oceanic Science Letters*, 6, 284–289, <https://doi.org/10.3878/j.issn.1674-2834.13.0042>, 2013.

813 Hussain, Md. and Mahmud, I.: pyMannKendall: a python package for non parametric Mann Kendall family of trend tests.,
814 *Journal of Open Source Software*, 4, 1556, <https://doi.org/10.21105/joss.01556>, 2019.

815 Ito, A. and Inatomi, M.: Water-use efficiency of the terrestrial biosphere: A model analysis focusing on interactions between
816 the global carbon and water cycles, *Journal of Hydrometeorology*, 13, 681–694, [https://doi.org/10.1175/JHM-D-10-](https://doi.org/10.1175/JHM-D-10-05034.1)
817 05034.1, 2012.

818 Jensen, J. D., Thurman, J., and Vincent, A. L.: *Lightning Injuries*, in: StatPearls, StatPearls Publishing, Treasure Island (FL),

819 2022.

820 Kaufman, Y. J., Tanré, D., Holben, B. N., Mattoo, S., Remer, L. A., Eck, T. F., Vaughan, J., and Chatenet, B.: Aerosol
821 Radiative Impact on Spectral Solar Flux at the Surface, Derived from Principal–Plane Sky Measurements, *Journal of*
822 *the Atmospheric Sciences*, 59, 635–646, [https://doi.org/10.1175/1520-0469\(2002\)059<0635:ARIOSS>2.0.CO;2](https://doi.org/10.1175/1520-0469(2002)059<0635:ARIOSS>2.0.CO;2), 2002.

823 Kelley, M., Schmidt, G. A., Nazarenko, L. S., Bauer, S. E., Ruedy, R., Russell, G. L., Ackerman, A. S., Aleinov, I., Bauer, M.,
824 Bleck, R., Canuto, V., Cesana, G., Cheng, Y., Clune, T. L., Cook, B. I., Cruz, C. A., Del Genio, A. D., Elsaesser, G. S.,
825 Faluvegi, G., Kiang, N. Y., Kim, D., Lacs, A. A., Leboissetier, A., LeGrande, A. N., Lo, K. K., Marshall, J., Matthews,
826 E. E., McDermid, S., Mezuman, K., Miller, R. L., Murray, L. T., Oinas, V., Orbe, C., García-Pando, C. P., Perlwitz, J.
827 P., Puma, M. J., Rind, D., Romanou, A., Shindell, D. T., Sun, S., Tausnev, N., Tsigaridis, K., Tselioudis, G., Weng, E.,
828 Wu, J., and Yao, M.-S.: GISS-E2.1: Configurations and Climatology, *Journal of Advances in Modeling Earth Systems*,
829 12, e2019 ms002025, <https://doi.org/10.1029/2019 ms002025>, 2020.

830 Koren, I., Kaufman, Y. J., Remer, L. A., and Martins, J. V.: Measurement of the Effect of Amazon Smoke on Inhibition of
831 Cloud Formation, *Science*, 303, 1342–1345, <https://doi.org/10.1126/science.1089424>, 2004.

832 Koren, I., Martins, J. V., Remer, L. A., and Afargan, H.: Smoke Invigoration Versus Inhibition of Clouds over the Amazon,
833 *Science*, 321, 946–949, <https://doi.org/10.1126/science.1159185>, 2008.

834 Krause, A., Kloster, S., Wilkenskjeld, S., and Paeth, H.: The sensitivity of global wildfires to simulated past, present, and
835 future lightning frequency, *Journal of Geophysical Research: Biogeosciences*, 119, 312–322,
836 <https://doi.org/10.1002/2013JG002502>, 2014.

837 Labrador, L. J., von Kuhlmann, R., and Lawrence, M. G.: The effects of lightning-produced NO_x and its vertical distribution
838 on atmospheric chemistry: sensitivity simulations with MATCH-MPIC, *Atmospheric Chemistry and Physics*, 5, 1815–
839 1834, <https://doi.org/10.5194/acp-5-1815-2005>, 2005.

840 Lal, D. M., Ghude, S. D., Mahakur, M., Waghmare, R. T., Tiwari, S., Srivastava, M. K., Meena, G. S., and Chate, D. M.:
841 Relationship between aerosol and lightning over Indo-Gangetic Plain (IGP), India, *Clim Dyn*, 50, 3865–3884,
842 <https://doi.org/10.1007/s00382-017-3851-2>, 2018.

843 Li, Z., Guo, J., Ding, A., Liao, H., Liu, J., Sun, Y., Wang, T., Xue, H., Zhang, H., and Zhu, B.: Aerosol and boundary-layer
844 interactions and impact on air quality, *National Science Review*, 4, 810–833, <https://doi.org/10.1093/nsr/nwx117>, 2017.

845 Liaskos, C. E., Allen, D. J., and Pickering, K. E.: Sensitivity of tropical tropospheric composition to lightning NO_x production
846 as determined by replay simulations with GEOS-5, *Journal of Geophysical Research*, 120, 8512–8534,
847 <https://doi.org/10.1002/2014JD022987>, 2015.

848 Liu, Y., Guha, A., Said, R., Williams, E., Lapierre, J., Stock, M., and Heckman, S.: Aerosol Effects on Lightning
849 Characteristics: A Comparison of Polluted and Clean Regimes, *Geophysical Research Letters*, 47, e2019GL086825,
850 <https://doi.org/10.1029/2019GL086825>, 2020.

851 Lopez, P.: A lightning parameterization for the ECMWF integrated forecasting system, *Monthly Weather Review*, 144, 3057–
852 3075, <https://doi.org/10.1175/MWR-D-16-0026.1>, 2016.

853 Manabe, S. and Wetherald, R. T.: The Effects of Doubling the CO₂ Concentration on the climate of a General Circulation
854 Model, *Journal of the Atmospheric Sciences*, 32, 3–15, <https://doi.org/10.1175/1520->
855 0469(1975)032<0003:TEODTC>2.0.CO;2, 1975.

856 van Marle, M. J. E., Kloster, S., Magi, B. I., Marlon, J. R., Daniau, A.-L., Field, R. D., Arneeth, A., Forrest, M., Hantson, S.,
857 Kehrwald, N. M., Knorr, W., Lasslop, G., Li, F., Mangeon, S., Yue, C., Kaiser, J. W., and van der Werf, G. R.: Historic
858 global biomass burning emissions for CMIP6 (BB4CMIP) based on merging satellite observations with proxies and fire
859 models (1750–2015), *Geosci. Model Dev.*, 10, 3329–3357, <https://doi.org/10.5194/gmd-10-3329-2017>, 2017.

860 McCaul, E. W., Goodman, S. J., LaCasse, K. M., and Cecil, D. J.: Forecasting lightning threat using cloud-resolving model
861 simulations, *Weather and Forecasting*, 24, 709–729, <https://doi.org/10.1175/2008WAF2222152.1>, 2009.

862 Meinshausen, M., Vogel, E., Nauels, A., Lorbacher, K., Meinshausen, N., Etheridge, D. M., Fraser, P. J., Montzka, S. A.,
863 Rayner, P. J., Trudinger, C. M., Krummel, P. B., Beyerle, U., Canadell, J. G., Daniel, J. S., Enting, I. G., Law, R. M.,
864 Lunder, C. R., O’Doherty, S., Prinn, R. G., Reimann, S., Rubino, M., Velders, G. J. M., Vollmer, M. K., Wang, R. H.
865 J., and Weiss, R.: Historical greenhouse gas concentrations for climate modelling (CMIP6), *Geoscientific Model*
866 *Development*, 10, 2057–2116, <https://doi.org/10.5194/gmd-10-2057-2017>, 2017.

867 Miller, R. L., Schmidt, G. A., Nazarenko, L. S., Tausnev, N., Bauer, S. E., DelGenio, A. D., Kelley, M., Lo, K. K., Ruedy, R.,
868 Shindell, D. T., Aleinoy, I., Bauer, M., Bleck, R., Canuto, V., Chen, Y., Cheng, Y., Clune, T. L., Faluvegi, G., Hansen,
869 J. E., Healy, R. J., Kiang, N. Y., Koch, D., Lacis, A. A., LeGrande, A. N., Lerner, J., Menon, S., Oinas, V., Pérez García-
870 Pando, C., Perlwitz, J. P., Puma, M. J., Rind, D., Romanou, A., Russell, G. L., Sato, M., Sun, S., Tsigaridis, K., Unger,
871 N., Voulgarakis, A., Yao, M.-S., and Zhang, J.: CMIP5 historical simulations (1850–2012) with GISS ModelE2, *Journal*
872 *of Advances in Modeling Earth Systems*, 6, 441–478, <https://doi.org/10.1002/2013ms000266>, 2014.

873 Murray, L. T.: Lightning NO_x and Impacts on Air Quality, *Current Pollution Reports*, 2, 115–133,
874 <https://doi.org/10.1007/s40726-016-0031-7>, 2016.

875 Ott, L. E., Pickering, K. E., Stenchikov, G. L., Allen, D. J., DeCaria, A. J., Ridley, B., Lin, R. F., Lang, S., and Tao, W. K.:
876 Production of lightning NO_x and its vertical distribution calculated from three-dimensional cloud-scale chemical
877 transport model simulations, *Journal of Geophysical Research Atmospheres*, 115, 4301,
878 <https://doi.org/10.1029/2009JD011880>, 2010.

879 Pinto, O.: Lightning and climate: A review, in: 2013 International Symposium on Lightning Protection (XII SIPDA), 2013
880 International Symposium on Lightning Protection (XII SIPDA), journalAbbreviation: 2013 International Symposium
881 on Lightning Protection (XII SIPDA), 402–404, <https://doi.org/10.1109/SIPDA.2013.6729250>, 2013.

882 Price, C. and Rind, D.: A simple lightning parameterization for calculating global lightning distributions, *Journal of*
883 *Geophysical Research*, 97, 9919–9933, <https://doi.org/10.1029/92JD00719>, 1992.

884 Price, C. and Rind, D.: What determines the cloud-to-ground lightning fraction in thunderstorms?, *Geophysical Research*
885 *Letters*, 20, 463–466, <https://doi.org/10.1029/93GL00226>, 1993.

886 Price, C. and Rind, D.: Possible implications of global climate change on global lightning distributions and frequencies, *Journal*

887 of Geophysical Research, 99, 823–833, <https://doi.org/10.1029/94jd00019>, 1994.

888 Rayner, N. A., Parker, D. E., Horton, E. B., Folland, C. K., Alexander, L. V., Rowell, D. P., Kent, E. C., and Kaplan, A.:
889 Global analyses of sea surface temperature, sea ice, and night marine air temperature since the late nineteenth century,
890 Journal of Geophysical Research: Atmospheres, 108, <https://doi.org/10.1029/2002jd002670>, 2003.

891 Ridley, B. A., Pickering, K. E., and Dye, J. E.: Comments on the parameterization of lightning-produced NO in global
892 chemistry-transport models, Atmospheric Environment, 39, 6184–6187,
893 <https://doi.org/10.1016/j.atmosenv.2005.06.054>, 2005.

894 Romps, D. M.: Evaluating the Future of Lightning in Cloud-Resolving Models, Geophysical Research Letters, 46, 14863–
895 14871, <https://doi.org/10.1029/2019GL085748>, 2019.

896 Romps, D. M., Seeley, J. T., Vollaro, D., and Molinari, J.: Projected increase in lightning strikes in the united states due to
897 global warming, Science, 346, 851–854, <https://doi.org/10.1126/science.1259100>, 2014.

898 Sato, M., Hansen, J. E., McCormick, M. P., and Pollack, J. B.: Stratospheric aerosol optical depths, 1850–1990, Journal of
899 Geophysical Research: Atmospheres, 98, 22987–22994, <https://doi.org/10.1029/93JD02553>, 1993.

900 Saunders, C. P. R., Keith, W. D., and Mitzeva, R. P.: The effect of liquid water on thunderstorm charging, Journal of
901 Geophysical Research: Atmospheres, 96, 11007–11017, <https://doi.org/10.1029/91JD00970>, 1991.

902 Schumann, U. and Huntrieser, H.: The global lightning-induced nitrogen oxides source, Atmospheric Chemistry and Physics,
903 7, 3823–3907, <https://doi.org/10.5194/acp-7-3823-2007>, 2007.

904 Sekiguchi, M. and Nakajima, T.: A k-distribution-based radiation code and its computational optimization for an atmospheric
905 general circulation model, Journal of Quantitative Spectroscopy and Radiative Transfer, 109, 2779–2793,
906 <https://doi.org/10.1016/j.jqsrt.2008.07.013>, 2008.

907 Sellar, A. A., Jones, C. G., Mulcahy, J. P., Tang, Y., Yool, A., Wiltshire, A., O’Connor, F. M., Stringer, M., Hill, R., Palmieri,
908 J., Woodward, S., de Mora, L., Kuhlbrodt, T., Rumbold, S. T., Kelley, D. I., Ellis, R., Johnson, C. E., Walton, J.,
909 Abraham, N. L., Andrews, M. B., Andrews, T., Archibald, A. T., Berthou, S., Burke, E., Blockley, E., Carslaw, K.,
910 Dalvi, M., Edwards, J., Folberth, G. A., Gedney, N., Griffiths, P. T., Harper, A. B., Hendry, M. A., Hewitt, A. J., Johnson,
911 B., Jones, A., Jones, C. D., Keeble, J., Liddicoat, S., Morgenstern, O., Parker, R. J., Predoi, V., Robertson, E., Siahnaa,
912 A., Smith, R. S., Swaminathan, R., Woodhouse, M. T., Zeng, G., and Zerroukat, M.: UKESM1: Description and
913 Evaluation of the U.K. Earth System Model, Journal of Advances in Modeling Earth Systems, 11, 4513–4558,
914 <https://doi.org/10.1029/2019ms001739>, 2019.

915 Shi, Z., Wang, H., Tan, Y., Li, L., and Li, C.: Influence of aerosols on lightning activities in central eastern parts of China,
916 Atmospheric Science Letters, 21, e957, <https://doi.org/10.1002/asl.957>, 2020.

917 Soden, B. J., Wetherald, R. T., Stenchikov, G. L., and Robock, A.: Global Cooling After the Eruption of Mount Pinatubo: A
918 Test of Climate Feedback by Water Vapor, Science, 296, 727–730, <https://doi.org/10.1126/science.296.5568.727>, 2002.

919 Sudo, K. and Akimoto, H.: Global source attribution of tropospheric ozone: Long-range transport from various source regions,
920 Journal of Geophysical Research Atmospheres, 112, <https://doi.org/10.1029/2006JD007992>, 2007.

921 Sudo, K., Takahashi, M., Kurokawa, J. I., and Akimoto, H.: CHASER: A global chemical model of the troposphere 1. Model
922 description, *Journal of Geophysical Research Atmospheres*, 107, ACH 7-1-ACH 7-20,
923 <https://doi.org/10.1029/2001JD001113>, 2002.

924 Takemura, T., Egashira, M., Matsuzawa, K., Ichijo, H., O'Ishi, R., and Abe-Ouchi, A.: A simulation of the global distribution
925 and radiative forcing of soil dust aerosols at the Last Glacial Maximum, *Atmospheric Chemistry and Physics*, 9, 3061–
926 3073, <https://doi.org/10.5194/acp-9-3061-2009>, 2009.

927 Tan, Y. B., Peng, L., Shi, Z., and Chen, H. R.: Lightning flash density in relation to aerosol over Nanjing (China), *Atmospheric*
928 *Research*, 174–175, 1–8, <https://doi.org/10.1016/j.atmosres.2016.01.009>, 2016.

929 Tang, Y., Rumbold, S., Ellis, R., Kelley, D., Mulcahy, J., Sellar, A., Walton, J., and Jones, C.: MOHC UKESM1.0-LL model
930 output prepared for CMIP6 CMIP historical, <https://doi.org/10.22033/ESGF/CMIP6.6113>, 2019.

931 Tost, H.: Chemistry–climate interactions of aerosol nitrate from lightning, *Atmospheric Chemistry and Physics*, 17, 1125–
932 1142, <https://doi.org/10.5194/acp-17-1125-2017>, 2017.

933 Veraverbeke, S., Finney, D., Werf, G. van der, Wees, D. van, Xu, W., and Jones, M.: Global attribution of anthropogenic and
934 lightning fires, *Copernicus Meetings*, <https://doi.org/10.5194/egusphere-egu22-1160>, 2022.

935 Wang, Q., Li, Z., Guo, J., Zhao, C., and Cribb, M.: The climate impact of aerosols on the lightning flash rate: Is it detectable
936 from long-term measurements?, *Atmospheric Chemistry and Physics*, 18, 12797–12816, [https://doi.org/10.5194/acp-](https://doi.org/10.5194/acp-18-12797-2018)
937 [18-12797-2018](https://doi.org/10.5194/acp-18-12797-2018), 2018.

938 Wang, Y., Wan, Q., Meng, W., Liao, F., Tan, H., and Zhang, R.: Long-term impacts of aerosols on precipitation and lightning
939 over the Pearl River Delta megacity area in China, *Atmospheric Chemistry and Physics*, 11, 12421–12436,
940 <https://doi.org/10.5194/acp-11-12421-2011>, 2011.

941 Watanabe, S., Hajima, T., Sudo, K., Nagashima, T., Takemura, T., Okajima, H., Nozawa, T., Kawase, H., Abe, M., Yokohata,
942 T., Ise, T., Sato, H., Kato, E., Takata, K., Emori, S., and Kawamiya, M.: MIROC-ESM 2010: Model description and
943 basic results of CMIP5-20c3m experiments, *Geoscientific Model Development*, 4, 845–872,
944 <https://doi.org/10.5194/gmd-4-845-2011>, 2011.

945 Wild, O.: Modelling the global tropospheric ozone budget: exploring the variability in current models, *Atmospheric Chemistry*
946 *and Physics*, 7, 2643–2660, <https://doi.org/10.5194/acp-7-2643-2007>, 2007.

947 Williams, Earle: <https://web.mit.edu/earlerw/www/index.html>, last access: 19 December 2022.

948 Williams, E. R., Weber, M. E., and Orville, R. E.: The relationship between lightning type and convective state of
949 thunderclouds, *Journal of Geophysical Research: Atmospheres*, 94, 13213–13220,
950 <https://doi.org/10.1029/JD094iD11p13213>, 1989.

951 Yang, X., Yao, Z., Li, Z., and Fan, T.: Heavy air pollution suppresses summer thunderstorms in central China, *Journal of*
952 *Atmospheric and Solar–Terrestrial Physics*, 95–96, 28–40, <https://doi.org/10.1016/j.jastp.2012.12.023>, 2013.

953 Yuan, T., Remer, L. A., Pickering, K. E., and Yu, H.: Observational evidence of aerosol enhancement of lightning activity and
954 convective invigoration, *Geophysical Research Letters*, 38, 4701, <https://doi.org/10.1029/2010GL046052>, 2011.

955 Zeng, G., Pyle, J. A., and Young, P. J.: Impact of climate change on tropospheric ozone and its global budgets, *Atmospheric*
956 *Chemistry and Physics*, 8, 369–387, <https://doi.org/10.5194/acp-8-369-2008>, 2008.

957 Zhao, P., Zhou, Y., Xiao, H., Liu, J., Gao, J., and Ge, F.: Total Lightning Flash Activity Response to Aerosol over China Area,
958 *Atmosphere*, 8, 26, <https://doi.org/10.3390/atmos8020026>, 2017.

959 Zhao, P., Li, Z., Xiao, H., Wu, F., Zheng, Y., Cribb, M. C., Jin, X., and Zhou, Y.: Distinct aerosol effects on cloud-to-ground
960 lightning in the plateau and basin regions of Sichuan, Southwest China, *Atmospheric Chemistry and Physics*, 20, 13379–
961 13397, <https://doi.org/10.5194/acp-20-13379-2020>, 2020.

962

963